A STUDY OF THE SYSTEM IDENTIFICATION FOR DAMAGE DETECTION

CONTRACT NO. DTFR 53-84-C-0029

NOVEMBER, 1986

FINAL REPORT

PREPARED FOR:

DEPARTMENT OF TRANSPORTATION
FEDERAL RAILROAD ADMINISTRATION

BY:

ADVANCED TECHNOLOGY AND RESEARCH, INC.
3933 SANDY SPRING ROAD
BURTONSVILLE, MD 20866

The frequency domain technique uses a Fast Fourier Transform (FFT) spectrum analyzer to calculate the system's transfer function, which requires the measurements of both the output response and the input. During the experiment a structure is randomly or impulsively excited and the transfer functions are averaged over the number of samples to eliminate as much noise as possible. An appropriate curve fitting algorithm is then used to extract the eigenvalues and eigenvectors from the transfer functions. Once these values have been extracted, the mathematical model, dynamic equations, of the system and the associated mass, stiffness, and damping matrices can be obtained by system identification technique.

Two new methods of identifying the existence and locations of cracks and other damages in continuous structural systems have been developed by investigating the changes in the mass and flexibility matrices respectively. The flow chart of the entire algorithm to identify a crack and its location is shown in Fig. 1

Both numerical and experimental tests were performed on cantilever beams and on an offshore platform scale model supported on soil foundation. The mass and flexibility matrices for each damaged and undamaged model are analyzed and the results used to illustrate the success of the procedure in detecting and locating damages in these structures.

CANTILEVER BEAM TEST - NUMERICAL RESULTS

Transfer functions of the steel cantilever beam model obtained from finite element method (using NASTRAN) were analyzed to obtain M by using the frequency domain curve fitting technique and the System Identification Algorithm.

A steel cantilever beam, whose geometry and its finite element model as shown in Fig. 2, has been analyzed. The beam is 1" wide, 12" long and 1/8" thick. Six measurement points are selected along the longitudinal direction. Cracks were simulated singulary at various positions. In each case, the crack lies between two sequential points and its length is 3/8" extending from the longitudinal edges to the crack tips. The elements in the mass matrix for the cut cases are divided by the corresponding values of the no cut case to give the mass ratio. A number of simulated cut cases were tested. In addition , three other test cases with varying length of cut were also investigated to demonstrate the correlation between damage size and system parameter. The cuts were made 3" from the lumped edge (in between points 5 and 6). The cuts were symmetrical, and were made as follows: 1st cut is 1/8", 2nd cut is 1/4" and the 3rd cut is 3/8". Fig. 3 describes the geometry, location of measurement points and the three different cut-length cases. The dynamic force was always applied at point 5.

MASS RATIO METHOD

Table 1 gives the results for Cut 3-4 Case (i.e., cut in the middle between points 3 and 4). It can be observed that the values in the (i = k = 4) block are greater than 1.Ø while the values in the rest of the matrix is less than 1.Ø except the diagonal terms. This provides a locater for the cut. For a better visual presentation, each row in the mass ratio matrix is plotted for each cut case. An example for cut 3-4 case is shown in Figure 4. It can be seen that the cut location has the narrowest upper-lower bound band and is therefore easily identified. Additional cases where the cut is not in the middle of two points but is closer to one point, have been analyzed. The effect of different boundary conditions, simply supported and fixed end conditions has also been investigated. The same regularity can be deduced from all above results. Fig. 5 is the mass ratio for Cut 4-5 case.

Comparing the mass ratio matrices of the three different depth cut cases, it is observed that the more serious the damage is the greater changes occur in mass matrix. These can be shown in Fig. 6 and 7 for the first cut and third cut situations.

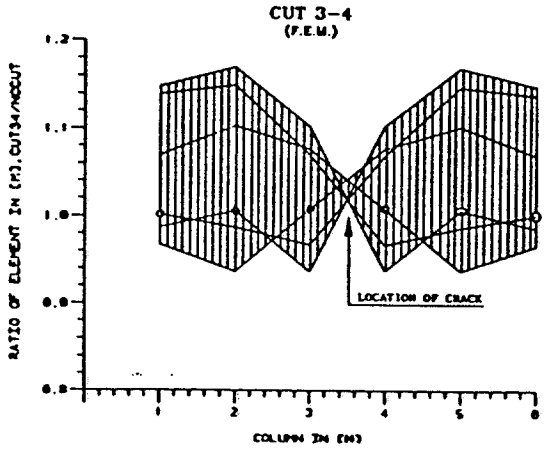

Figure 4 2-D Plot for the Mass Ratio Matrix of Cut 3-4 (F.E.M.)

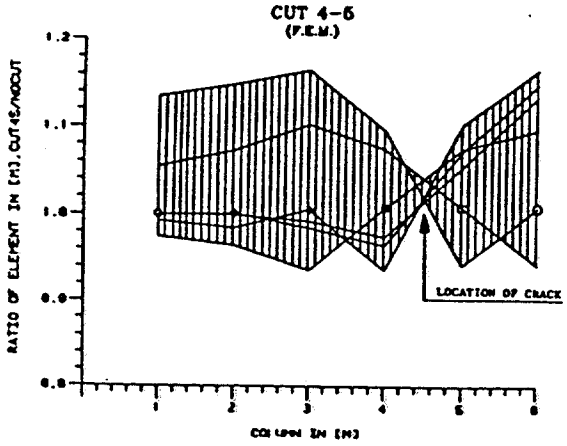

Figure 5 2-D Plot for the Mass Ratio Matrix of Cut 4-5 (F.E.M.)

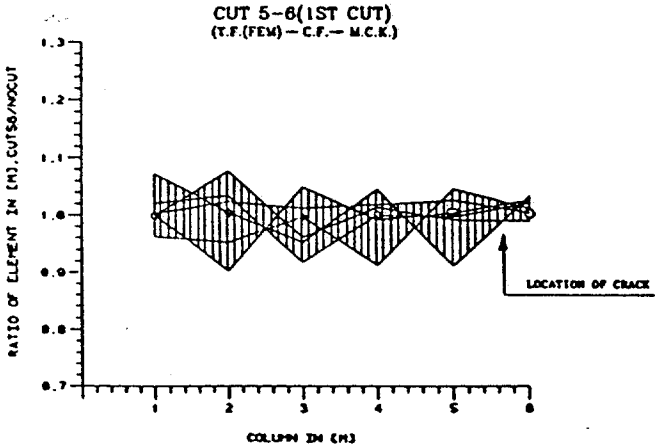

Figure 6 2-D Plot for the Mass Ratio Matrix of Cut 5-6 (1st Cut)

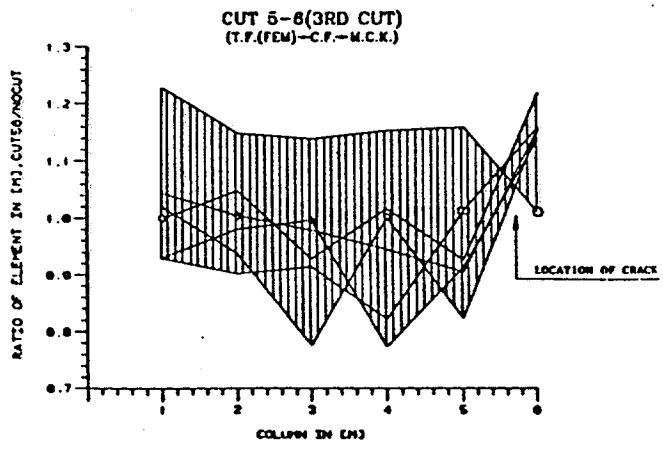

Figure 7 2-D Plot for the Mass Ratio Matrix of Cut 5-6 (3rd Cut)

FLEXIBILITY METHOD

In our theoretical study, see reference (5), it was shown that the diagonal elements of the flexibility matrix [F] , which is the inverse of [K] , deviate in an orderly fashion with respect to the location of the damage. To demonstrate its use in locating the crack, the flexibility matrix [F] is extracted by the System Identification Technique, for various cut cases shown as in Fig. 3. Fig. 8 shows the diagonal term changes in [F].

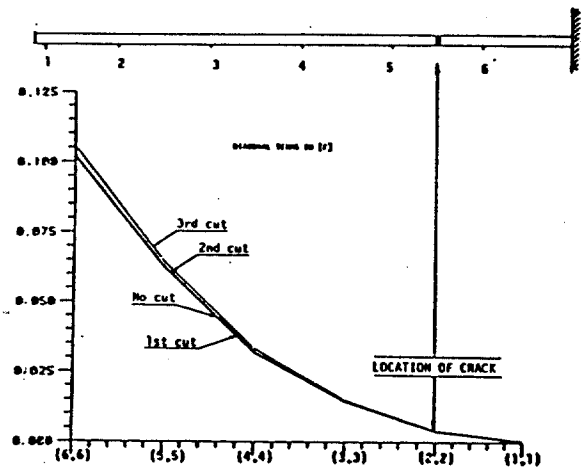

Figure 8 Diagonal Terms Change in Flexibility Matrix

As the cracks were introduced, all the diagonal terms in [F] beginning from F22 to F66 increased in value. According to the Flexibility Matrix Theory the cut is predicted and lies in segment 2 (between points 5 and 6).

CANTILEVER BEAM TEST - EXPERIMENTAL RESULTS

An experiment has been conducted using an aluminum beam. Its geometry, and location of the measurement stations are shown in Fig. 9. The beam is 1" wide, 19.5" long and 1/4" thick. Saw cuts were introduced between points 4 and 5. The cut is symmetrical, and 1/4" long starting from the edges. Two additional saw cuts were made 1/16" deep from the bottom and the top planes. An impulse hammer with force sensor and accelerometers were used to provide and pick up the forcing function signals at point 5 and the response signals from six selected points. The transfer functions from the impact point to any accelerometer point were obtained by the Nicolet FFT analyzer. Fig. 10 is the mass ratio matrix changes obtained from the experimental results. Cracks between points 4 and 5 are still identifiable, even though the mass ratio values showed more scatter than in the numerical case. Fig. 11 is the flexibility matrix changes obtained from the experimental results. The on-set of the monotonic divergence between drastic cut and no cut cases indicates that the cut location is at segment 3, between points 4 and 5.

OFFSHORE PLATFORM TEST - NUMERICAL RESULTS

A 1/14 scale steel model simulating an offshore platform in the Gulf of Mexico was used to demonstrate the application of the mass ratio and flexibility methods to detect and locate damages in complex structures. The geometry and dimensions are shown in Fig. 12. The platform model was supported on four steel piles with 2.5" outside diameter and 7 ft. length which were embedded in soil foundation. Two types of selected point distribution were considered (see Figs. 13 and 14). The first one was the line condensation, the type which has 7 selected points, 6 of them lined along one leg. The second type was the plane condensation which has 9 selected points, 8 of them were arranged in one plane. A through cut damage was created at the third level horizontal bracing in both models.

A finite element model was developed using the NASTRAN structure analysis computer code. The top plate was modelled with quadrilateral plate elements which account for bending as well as membrane stresses. All cross members were modelled as beam elements to account for bending in the members. The soil foundation was assumed to be a Winkler foundation which was modelled with suitable elastic spring and dashpot elements. Eight pairs of springs, one for each of two horizontal directions of motion, were attached to beam elements that represent each of the four piles embedded in soil.

The damping values, C, of all the dashpots attached to the pile elements were determined to be 2 lb/in/sec.

Each model consists of 158 grid points, 153 CBAR, 48 CQUAD2, 4 CONM2 elements, 64 linear elastic spring and 64 dashpots.

MASS RATIO METHOD - LINE CONDENSATION CASE

Fig. 15 is the plot of the diagonal terms in the mass ratio matrix. The most influenced elements in the matrix are (3,3) and (4,4), with (4,4) the maximum. This is reasonable since only points 3 and 4 have a bar member directly connected to the damage. Similar to the cantilever beam case when the damage is between points 3 and 4, the element (4,4) has the maximum value in the diagonal of the mass ratio matrix. Therefore, the procedures to identify the crack damage location in line condensation case are

- Determine the two most influenced elements and the positions of the related points from the diagonal terms in the mass ratio matrix.
- The crack should be located on members which are connected to both identified points.

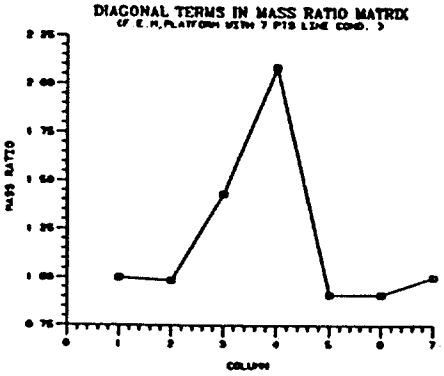

Figure 15 Diagonal Terms of Mass Ratio Matrix (Platform with Line Condensation)

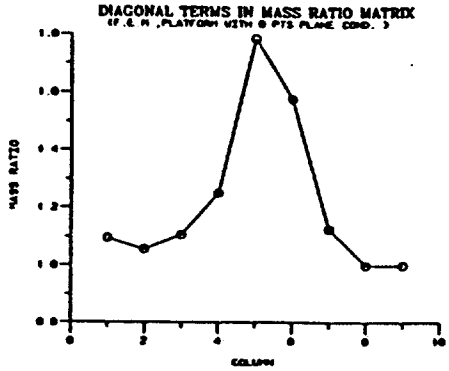

Figure 16 Diagonal Terms of Mass Ratio Matrix (Platform with Plane Condensation)

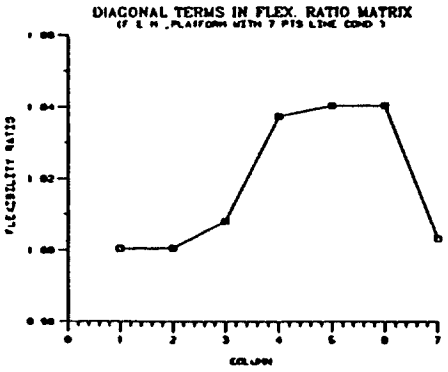

Figure 17 Diagonal Terms of Flex. Ratio Matrix (Platform with Line Condensation)

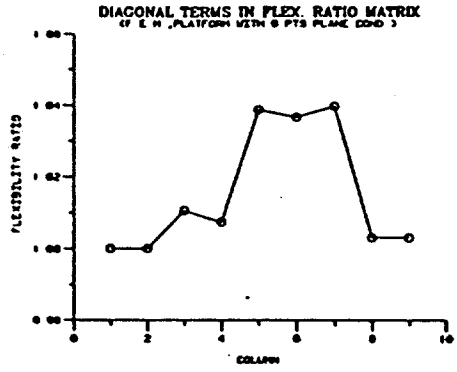

Figure 18 Diagonal Terms of Flex. Ratio Matrix (Platform with Plane Condensation)

OFFSHORE PLATFORM TEST - EXPERIMENTAL RESULTS

An 1:14 scale model of an offshore platform structure supported on steel frame was set up on concrete foundation outside the robotics laboratory in the University of Maryland for damage tests. Its geometry is described in Fig. 12. Fig. 19 is the picture of 1/14 scale offshore platform model with 31.5 inch long steel frame. Fig. 20 is the detail picture of the connection between main legs and the embedded steel frame. Figs. 21 and 22 are the front and side views of model sitting inside the dug hole which is 7 feet by 7 feet. The frame bracket tighten to the brick wall is the support for pendulum equipped with hammer and forcd transducer at the end. Figs. 23 and 24 are the pictures of model after concrete is poured into the dug hole. Eleven accelerometer positions were selected in the experimental model. They are labeled point 1 through 11, and the accelerometers along the same leg are arranged in the same direction. The positions of the accelerometers are shown in Fig. 25.

The pendulum was set up to provide impact excitation at the point No. 11. The responses at all accelerometer positions were monitored before and after system was changed. Two kinds of experiments have been performed, ie. system with added weight and system with damages.

SYSTEM WITH ADDED WEIGHT - As shown in Fig. 25, 33 lb. weight was

added at point No. 10 on the top plate. The purpose of this experiment is to investigate how the mathematical model changes, especially mass matrix, after added weight was aplied to the system. For calculation efficiency, the system was simplified as a 5 DOF, including points 2, 4, 6, 8 and 11. Fig. 26 is the plot for diagonal terms in mass ratio matrix between baseline and added weight cases. It shows that the closer the points to the added weight position, the greater their masses have changed, e.g. points 8 and 11. This is a reasonable trend as expected.

SYSTEM WITH DAMAGES - Three stages of damage were introduced to the structure, refer to fig. 27. The first stage damage was a saw cut at the middle point of the horizontal connecting beam between positions 3 and 4, and the cut was one third deep through the diameter of the beam. The second stage damage was a two third deep through the diameter of the beam. The third stage damage was a complete through cut at the same location. Therefore, there are four senarios analyzed: baseline, first stage, second stage, and third stage damages. Fig. 28-32 are the pictures of the vibration test instruments and the horizontal beam with damage in four senarios. Fig. 33-47 are the transfer functions at positions 2, 4, 6, 8 and 11 for the baseline, second and third senarios. The spectra indicate that there are distinct frequency shifts and changes in peak amplitudes before and after damage.

System parameters corresponding to different damage stage have been analyzed and the results are described as followings.

CONCLUSIONS

The System Identification Technique for characterizing the system through [M] , [C] and [K] matrices by use of the frequency response under single loading has been developed. Reasonable results obtained from tests in continuous systems successfully verified the algorithm.

The crack location in the structural system can be identified by analyzing the changes in the mass ratio matrix or the diagonal terms in the flexibility matrix.

Based on the present study, the mass ratio matrix is more sensitive than the flexibility matrix to damage in the structure.

The relative severity of the damage can also be verified by observing the behavior of the mass ratio plots. A more severe cut shows a more scattered upper-lower bound and a more distinct cut location. Similarly, in the flexibility matrix plots, the more severe cut shows more deviation from the baseline.

FIG. 21 1/14 SCALE OFFSHORE PLATFORM MODEL SITTING INSIDE THE DUG HOLE (SIDE VIEW)

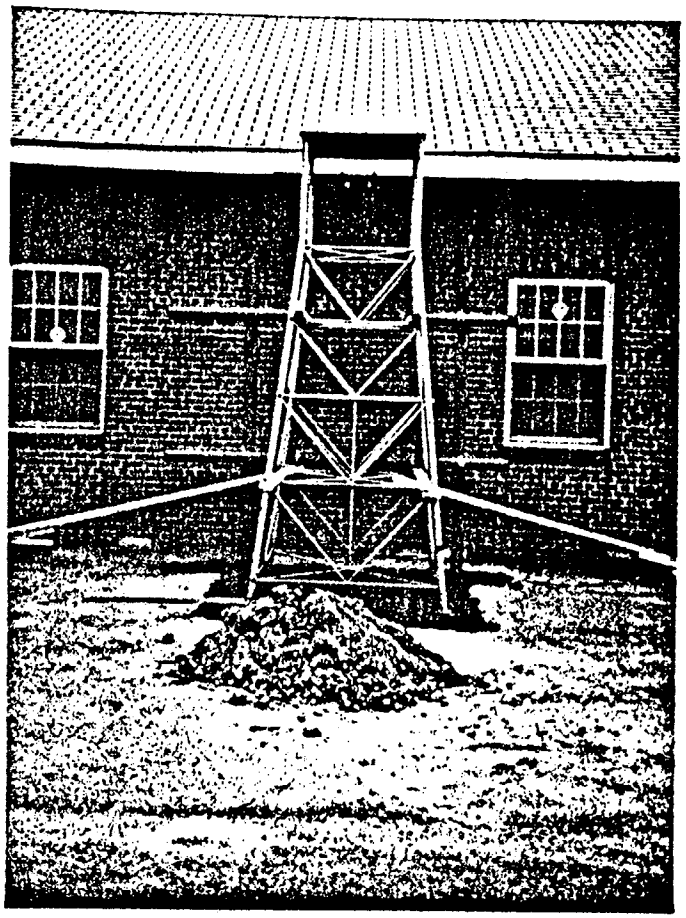

FIG. 22 1/14 SCALE OFFSHORE PLATFORM MODEL SITTING INSIDE THE DUG HOLE (FRONT VIEW)

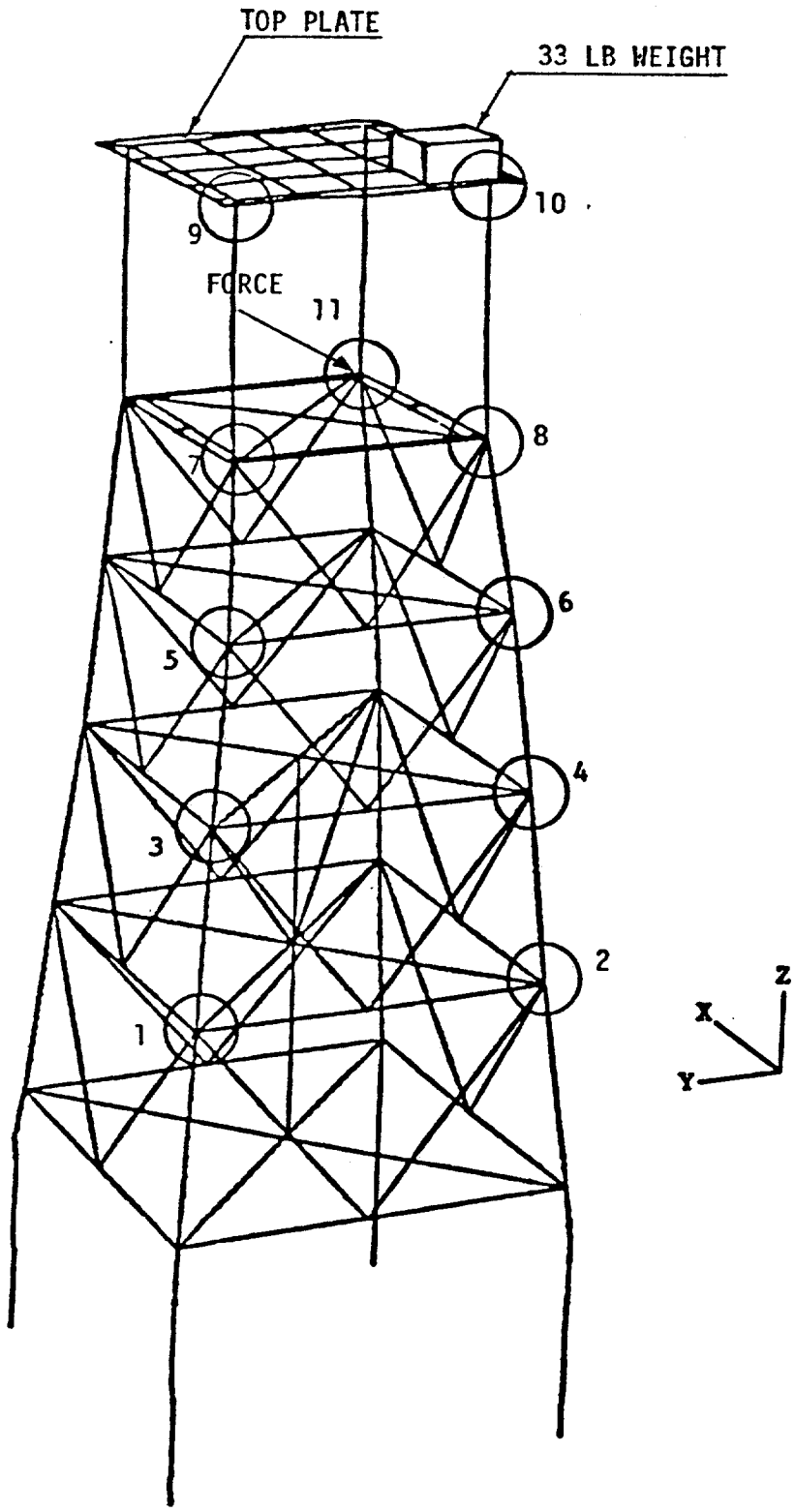

FIG. 25 1/14 SCALE OFFSHORE PLATFORM EXPERIMENTAL MODEL WITH 33 LB. WEIGHT ON THE TOP PLATE

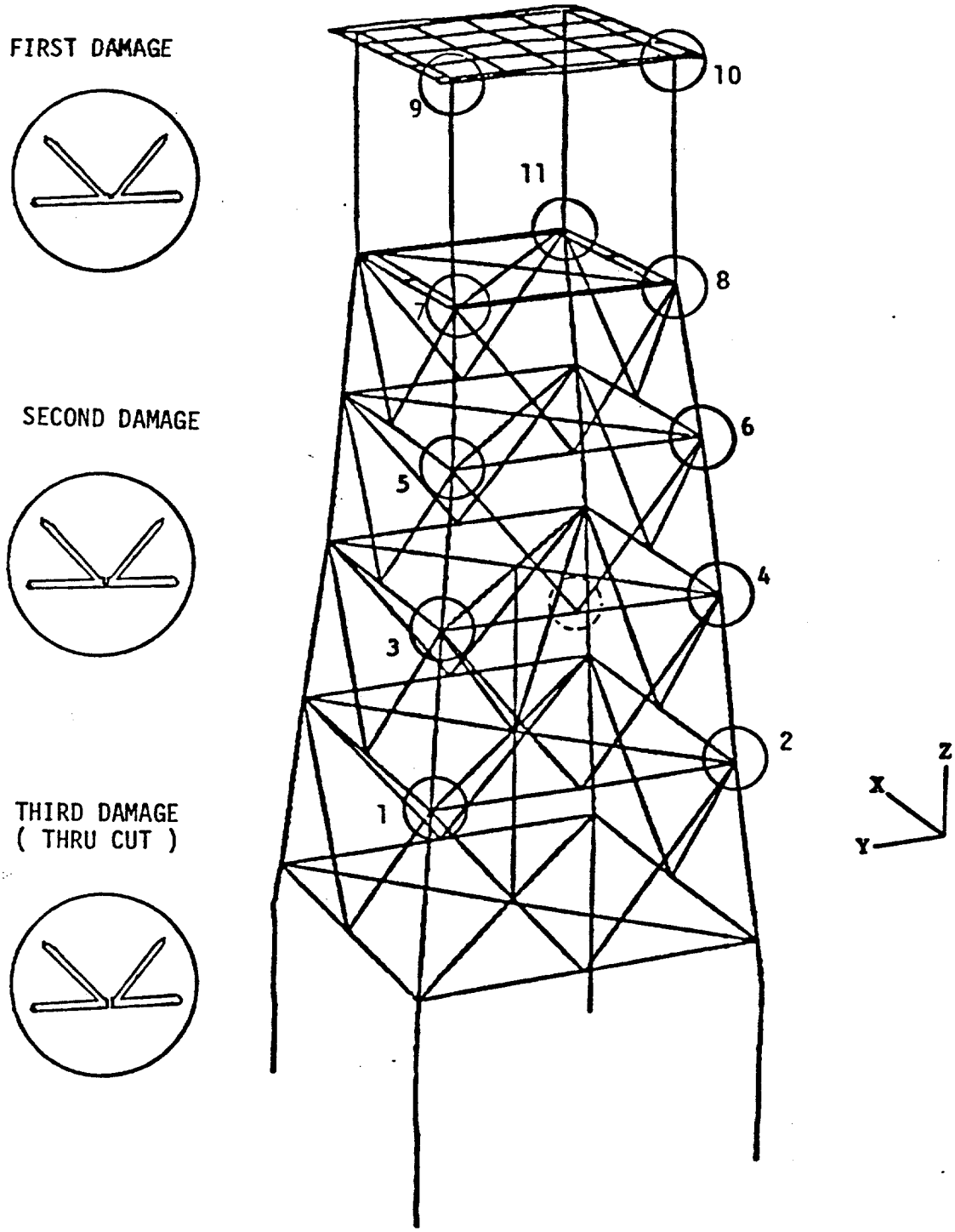

FIG. 27 THE MEASUREMENT POINT NUMBERING AND THE CRACK LOCATION FOR 1/14 SCALE OFFSHORE PLATFORM EXPERIMENTAL MODEL

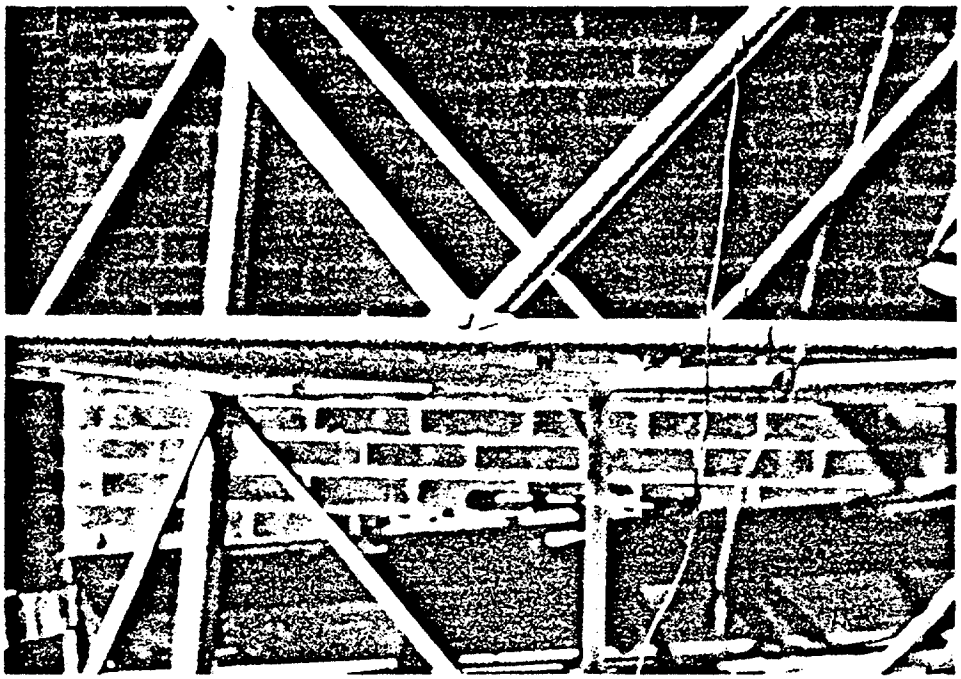

FIG. 29 THE CROSS BEAM FOR BASELINE CASE

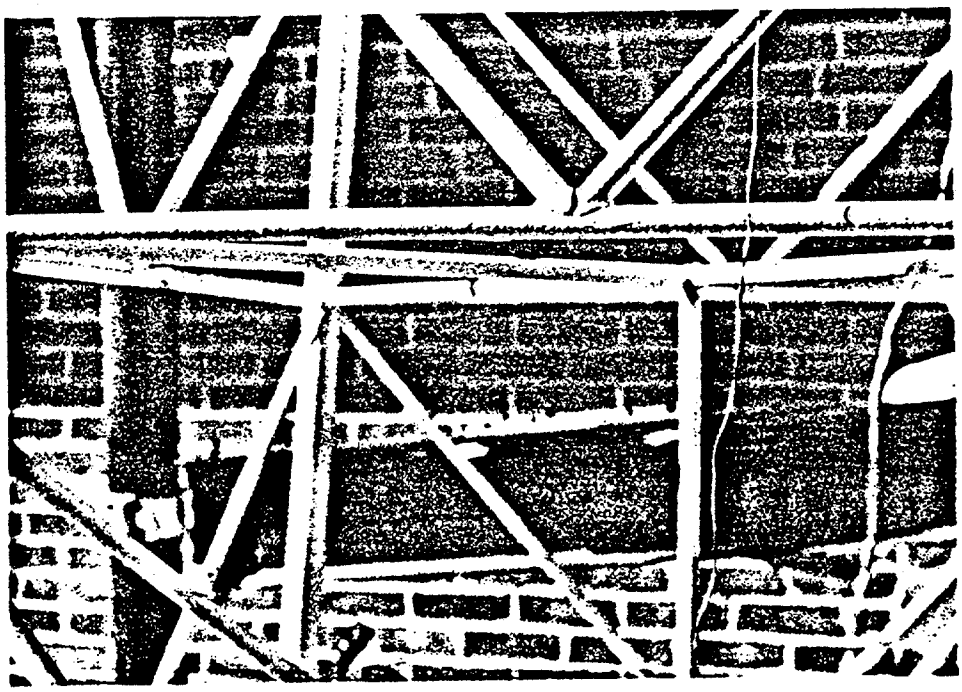

FIG. 30 THE FIRST DAMAGE CASE
(1/3 DEPTH CUT ON THE CROSS BEAM)

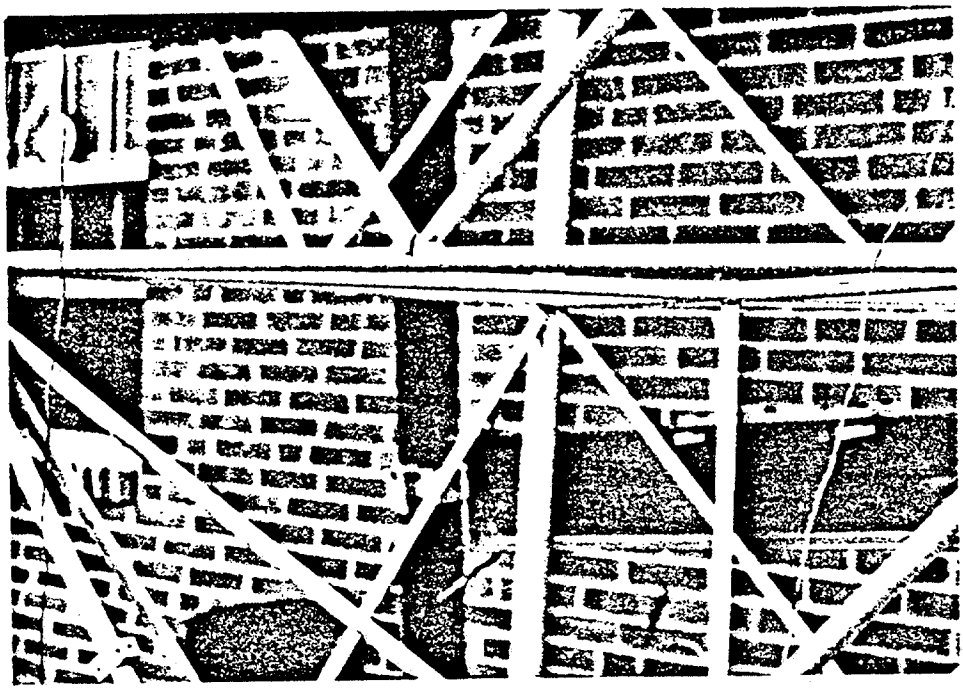

FIG. 31 THE SECOND DAMAGE CASE
(2/3 DEPTH CUT ON THE CROSS BEAM)

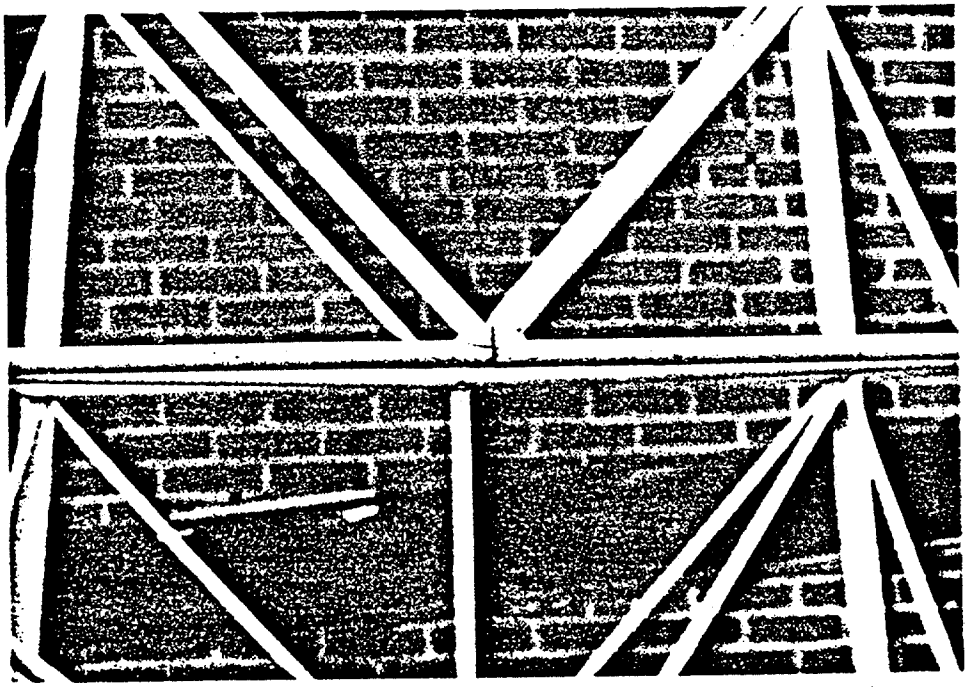

FIG. 32 THE THIRD DAMAGE CASE
(THROUGH CUT ON THE CROSS BEAM)

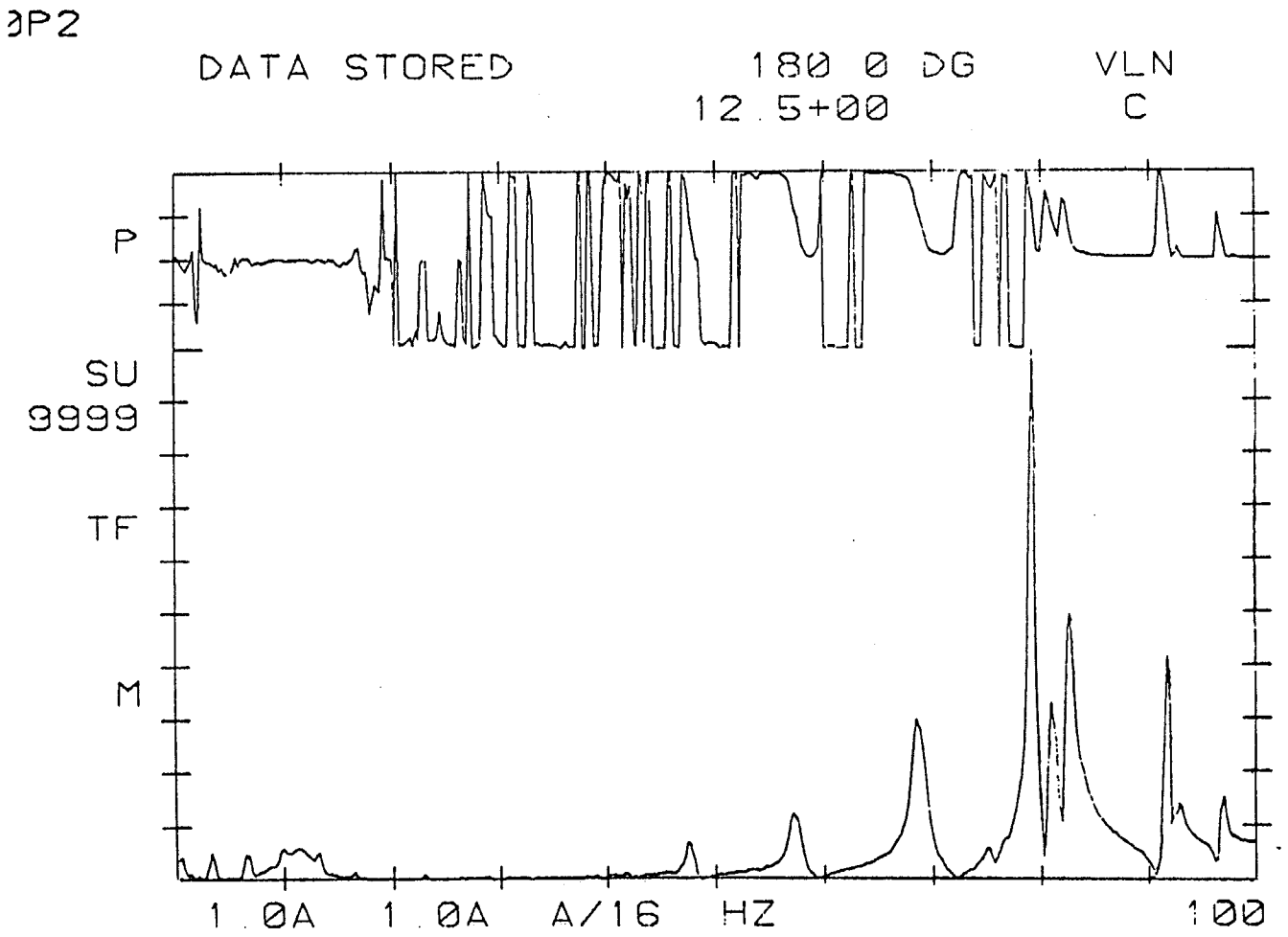

FIG. 33 TRANSFER FUNCTION FOR POINT NO. 2 AT NO DAMAGE CASE

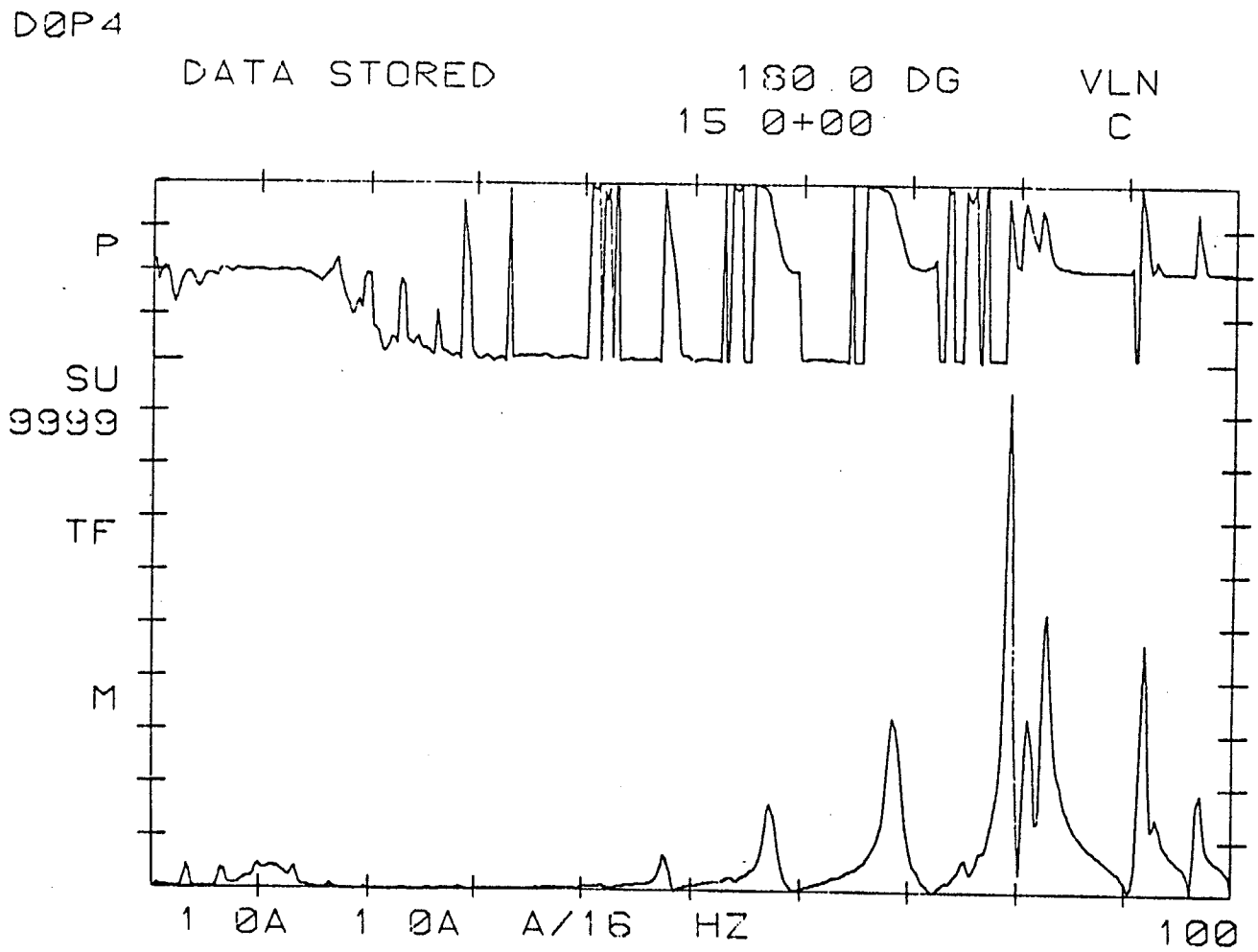

FIG. 34 TRANSFER FUNCTION FOR POINT NO. 4 AT NO DAMAGE CASE

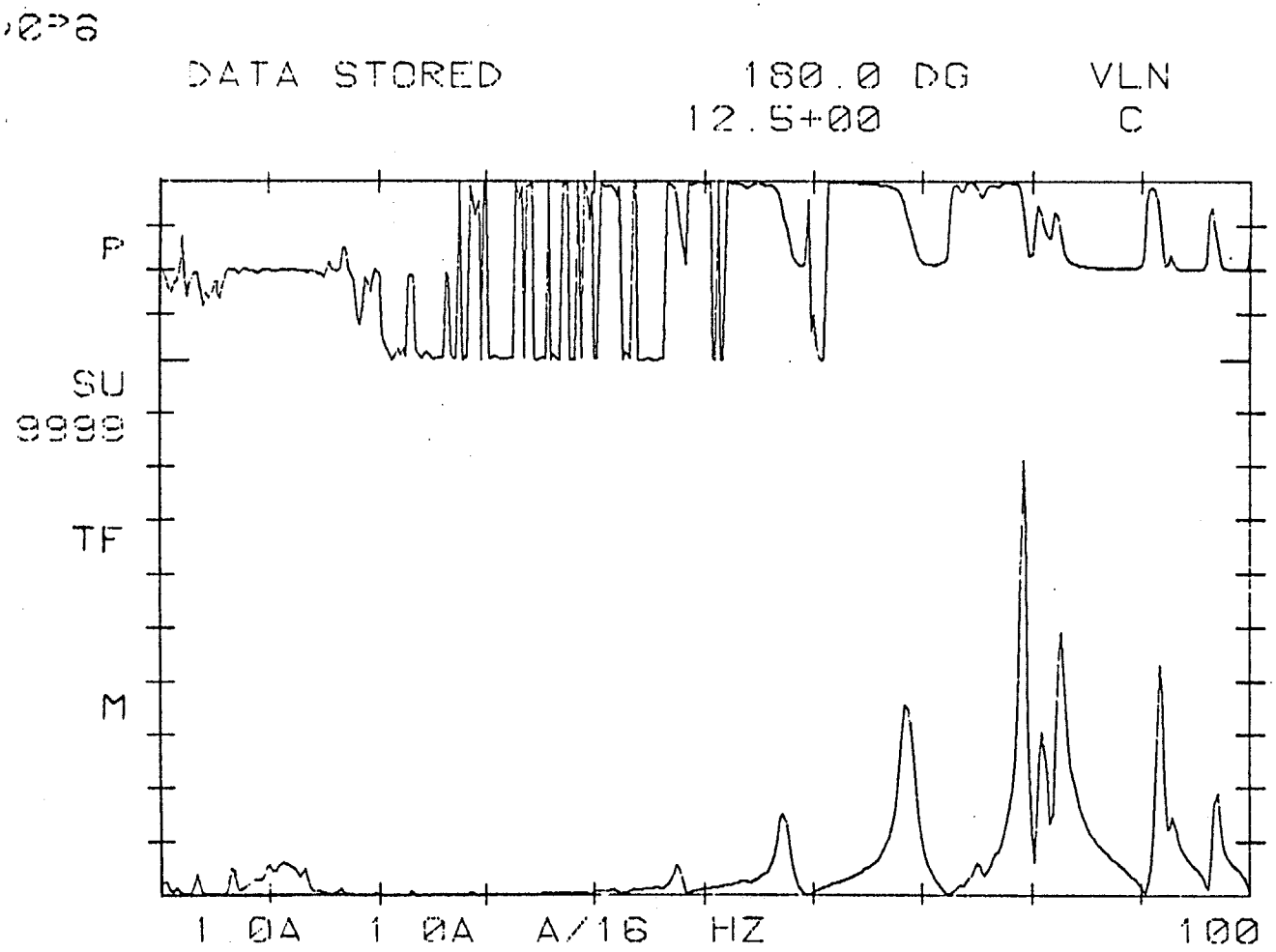

FIG. 35 TRANSFER FUNCTION FOR POINT NO. 6 AT NO DAMAGE CASE

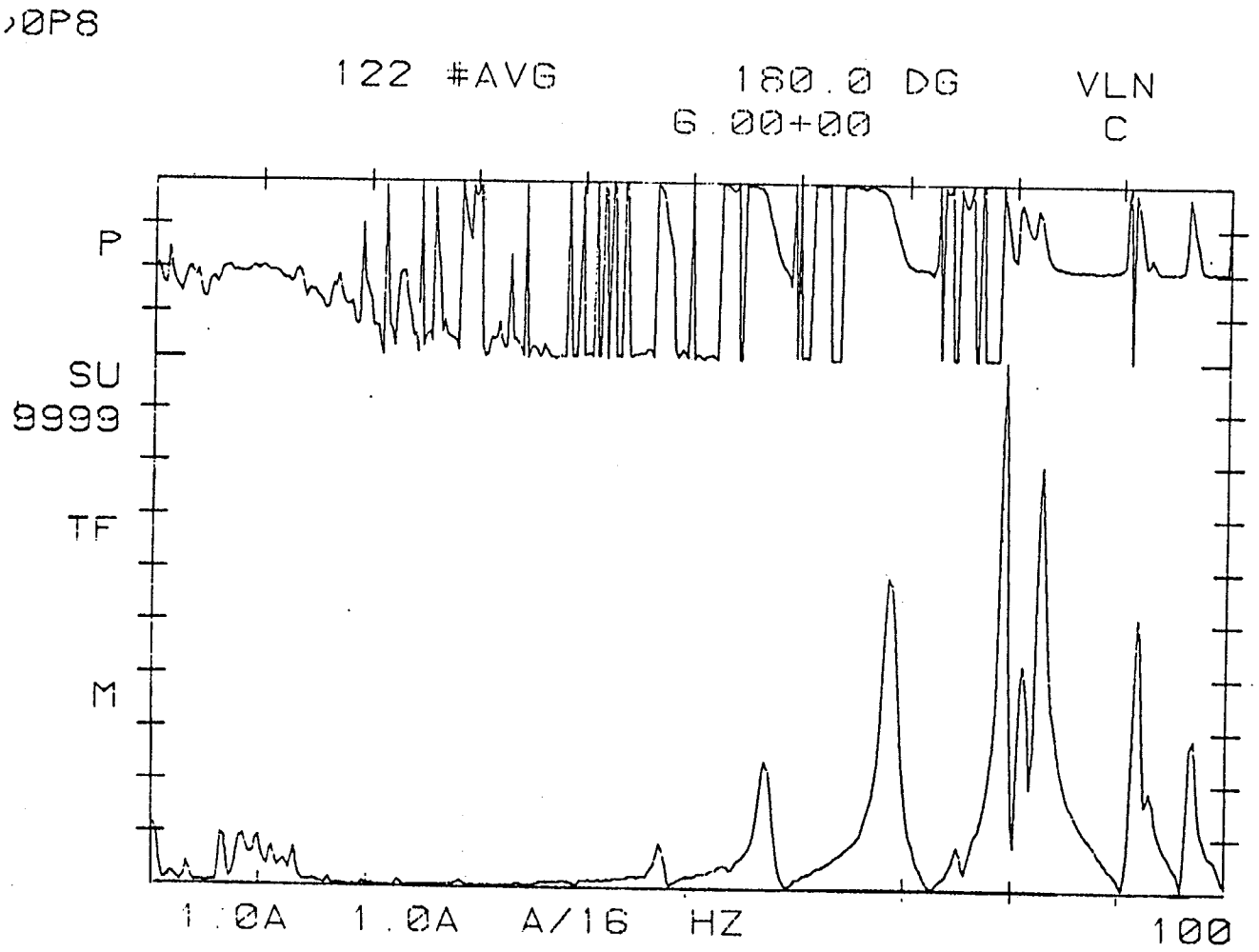

FIG. 36 TRANSFER FUNCTION FOR POINT NO. 8 AT NO DAMAGE CASE

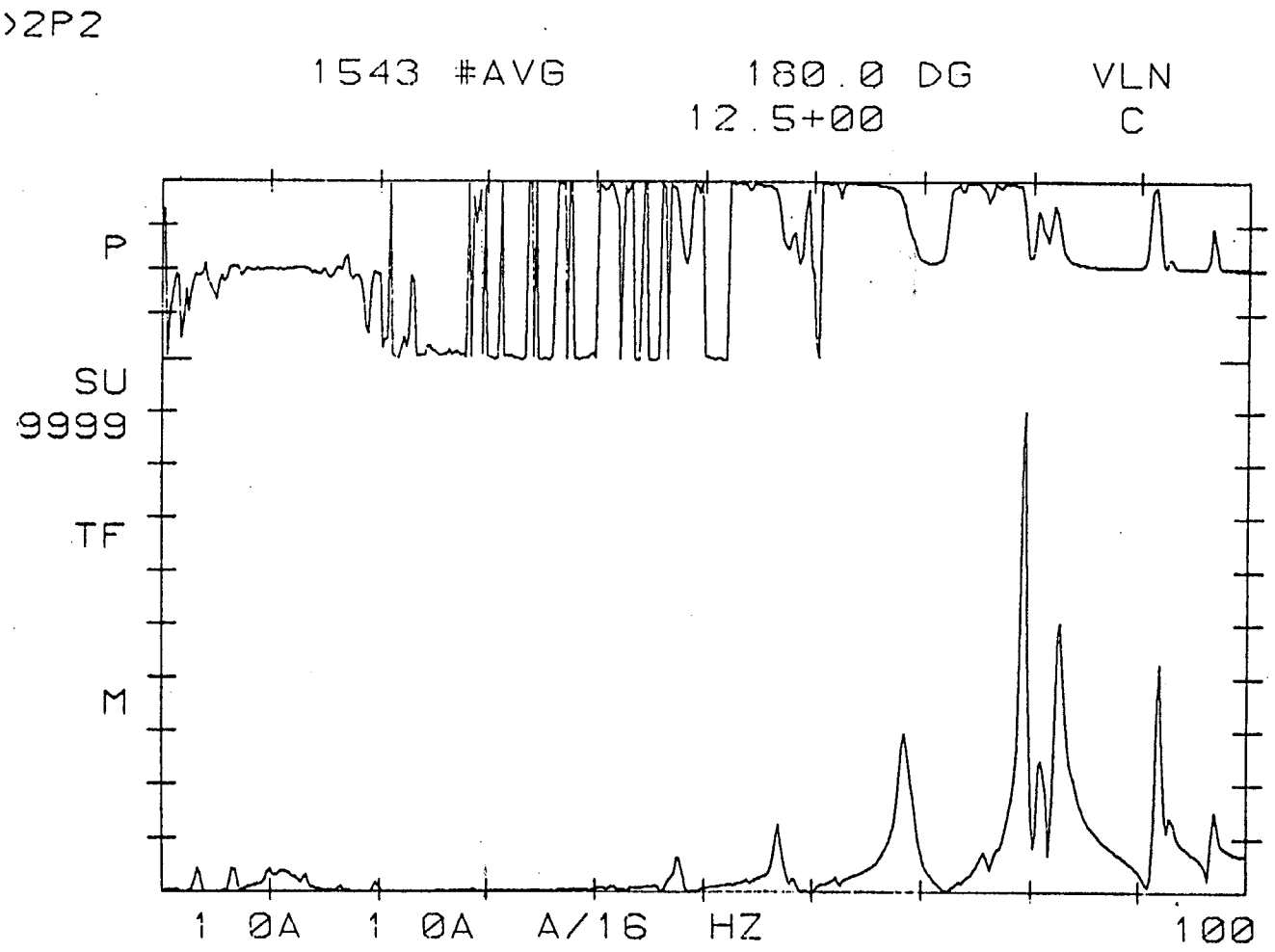

FIG. 38 TRANSFER FUNCTION FOR POINT NO. 2 AT THE 2ND DAMAGE CASE

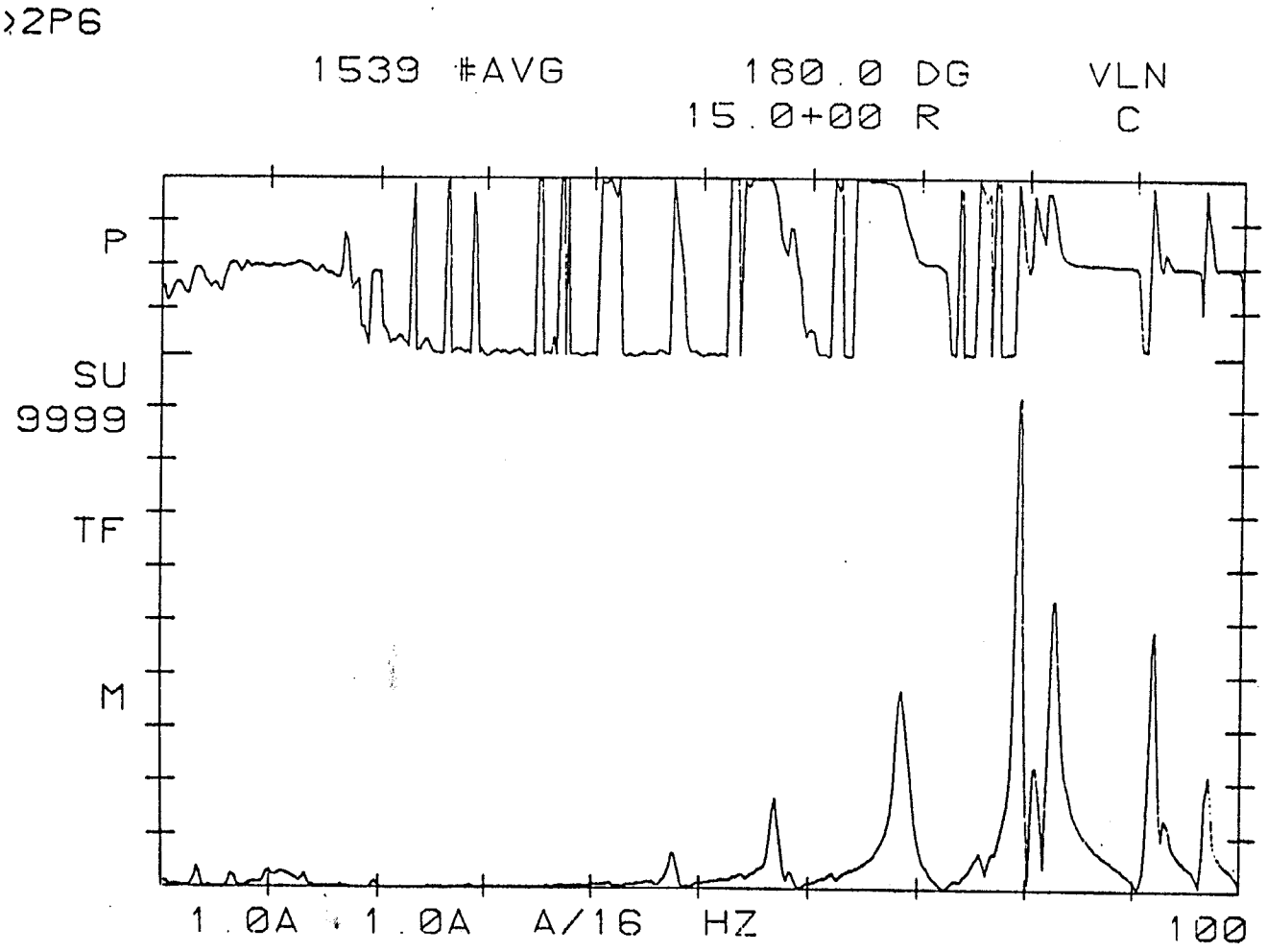

FIG. 40 TRANSFER FUNCTION FOR POINT NO. 6 AT THE 2ND DAMAGE CASE

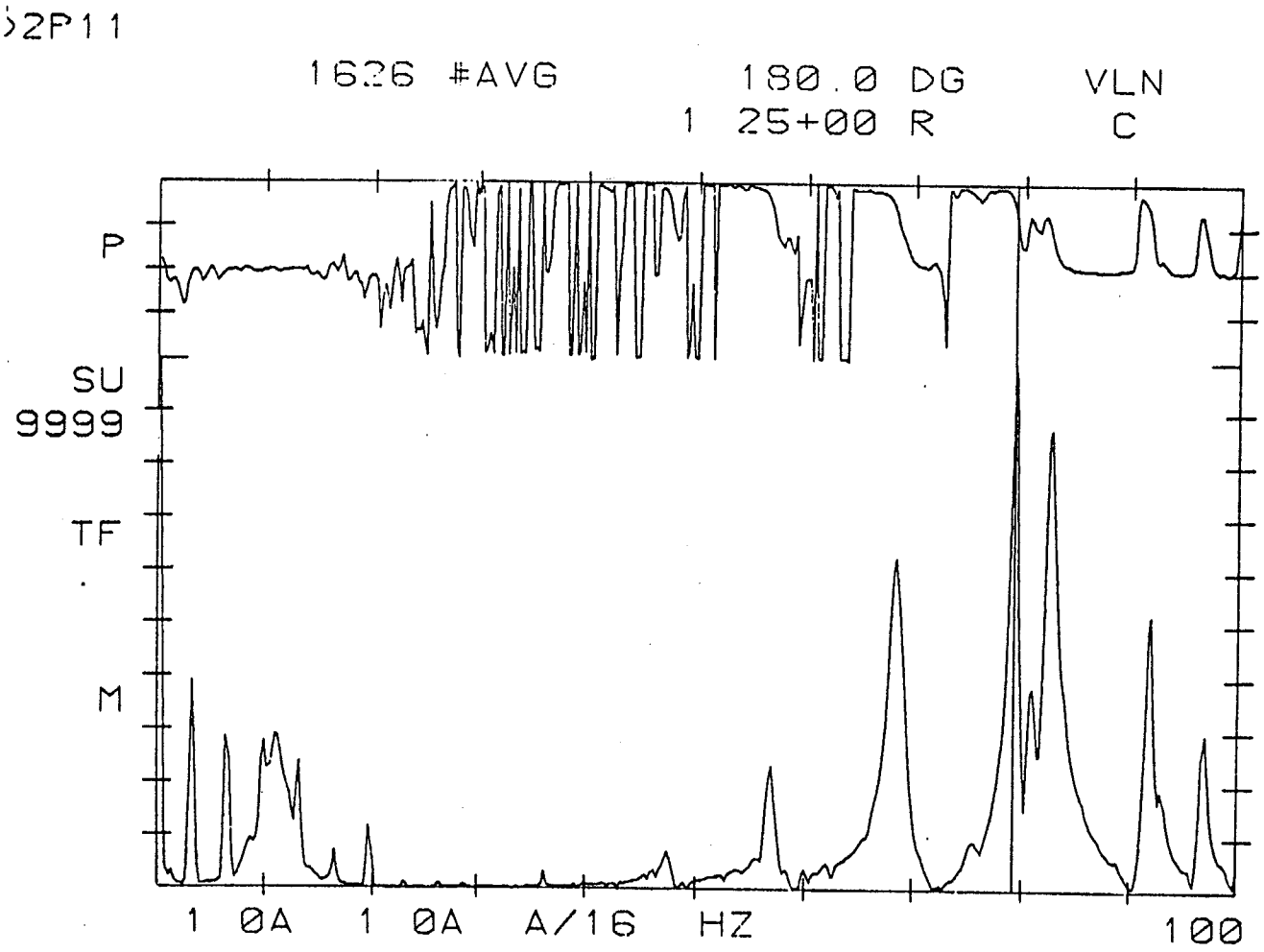

FIG. 42 TRANSFER FUNCTION FOR POINT NO. 11 AT THE 2ND DAMAGE CASE

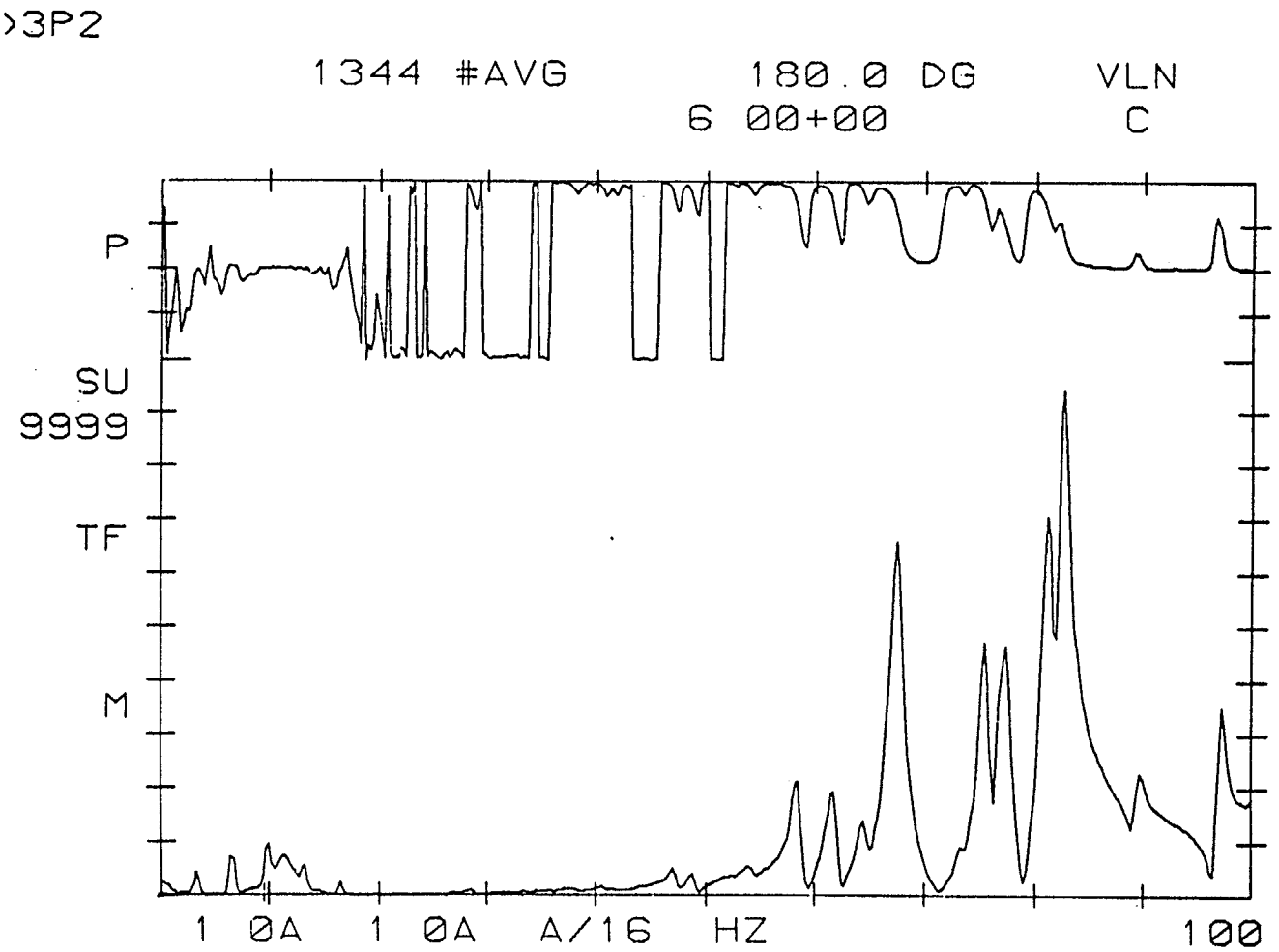

FIG. 43 TRANSFER FUNCTION FOR POINT NO. 2 AT THE 3RD DAMAGE CASE

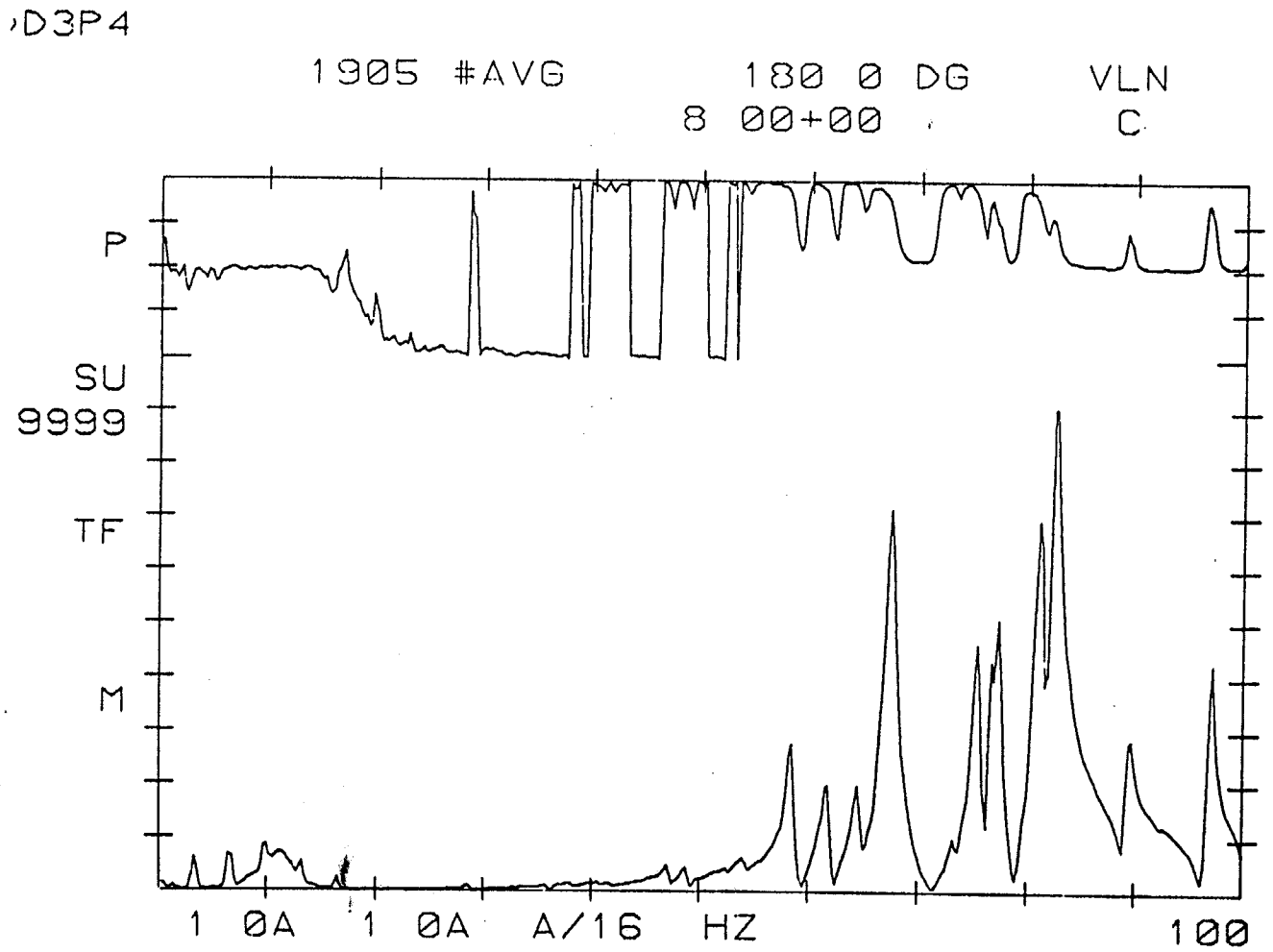

FIG. 44 TRANSFER FUNCTION FOR POINT NO. 4 AT THE 3RD DAMAGE CASE

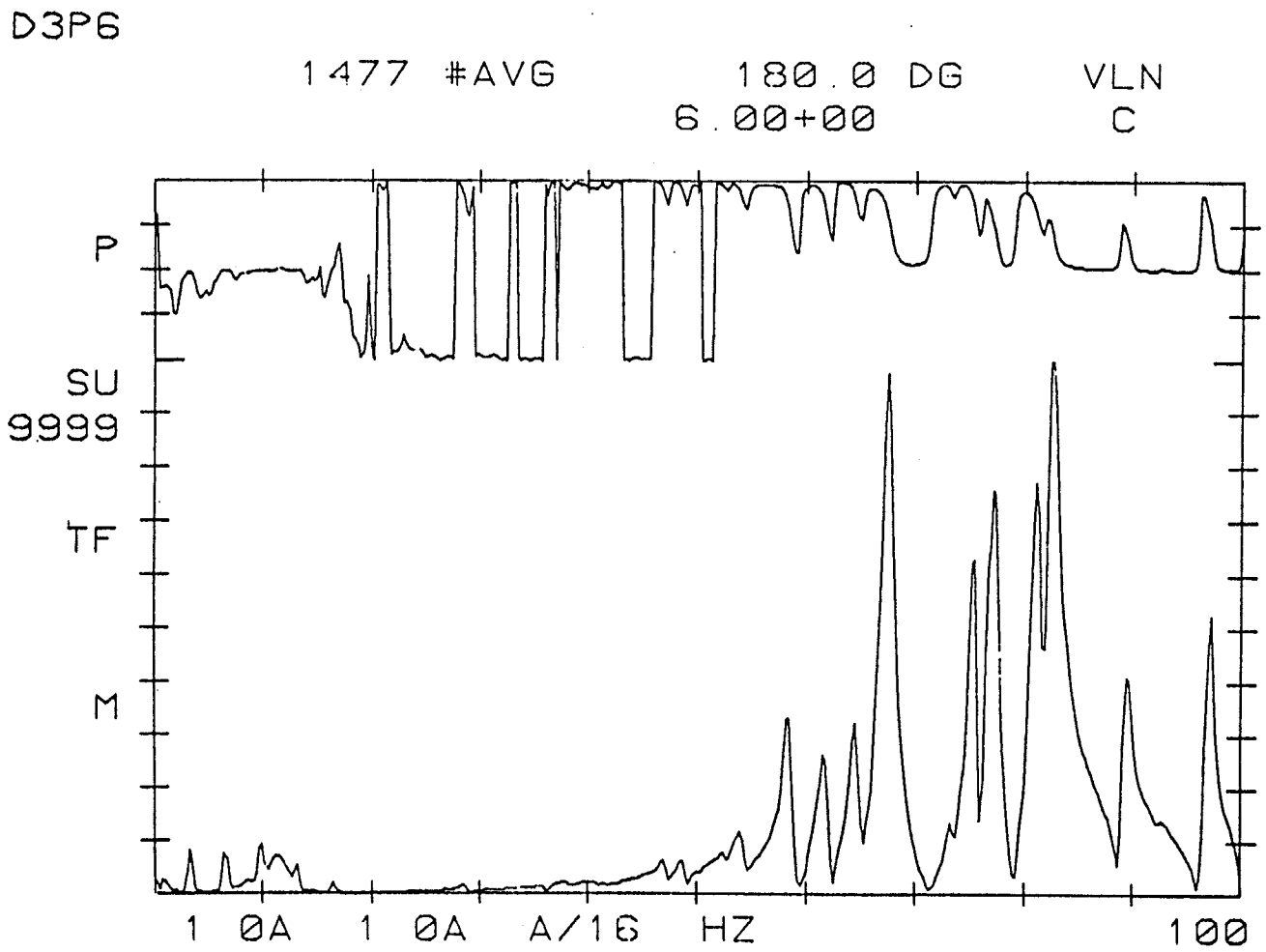

FIG. 45 TRANSFER FUNCTION FOR POINT NO. 6 AT THE 3RD DAMAGE CASE

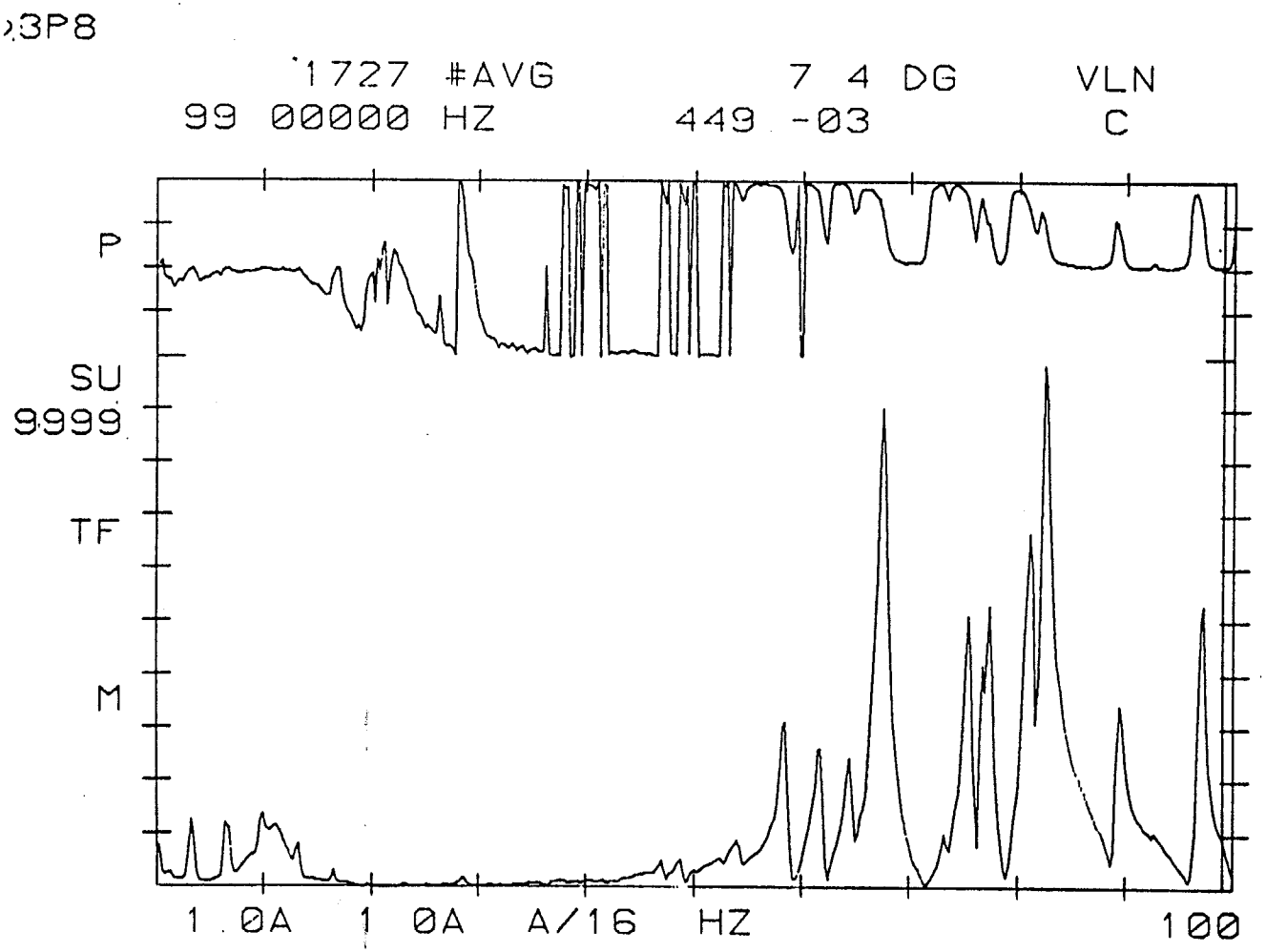

FIG. 46 TRANSFER FUNCTION FOR POINT NO. 8 AT THE 3RD DAMAGE CASE

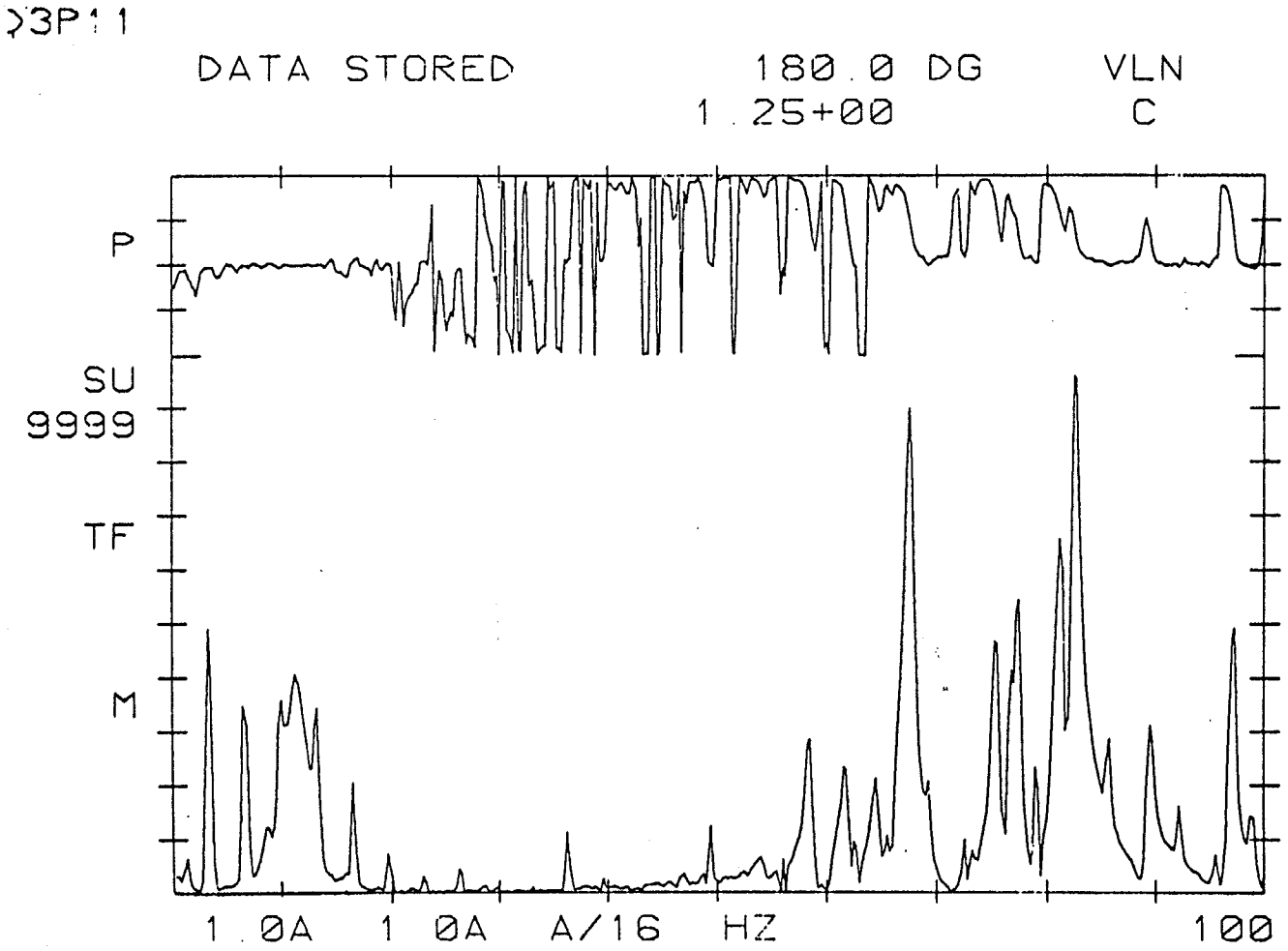

FIG. 47 TRANSFER FUNCTION FOR POINT NO. 11 AT THE 3RD DAMAGE CASE

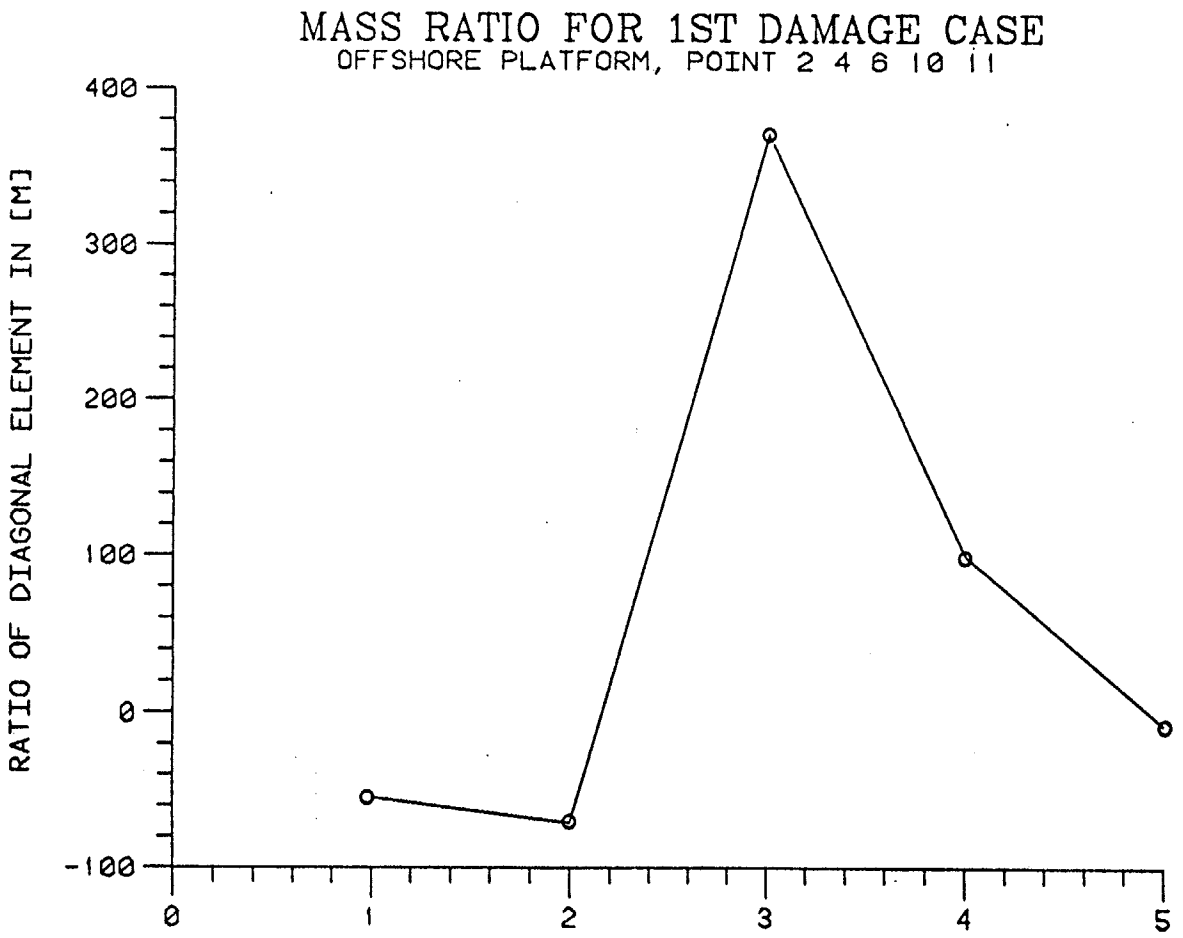

FIG. 48 THE DIAGONAL TERMS IN MASS RATIO MATRIX FOR THE FIRST DAMAGE CASE OF 1/14 SCALE OFFSHORE PLATFORM EXPERIMENTAL MODEL WITH CONCRETE FOUNDATION

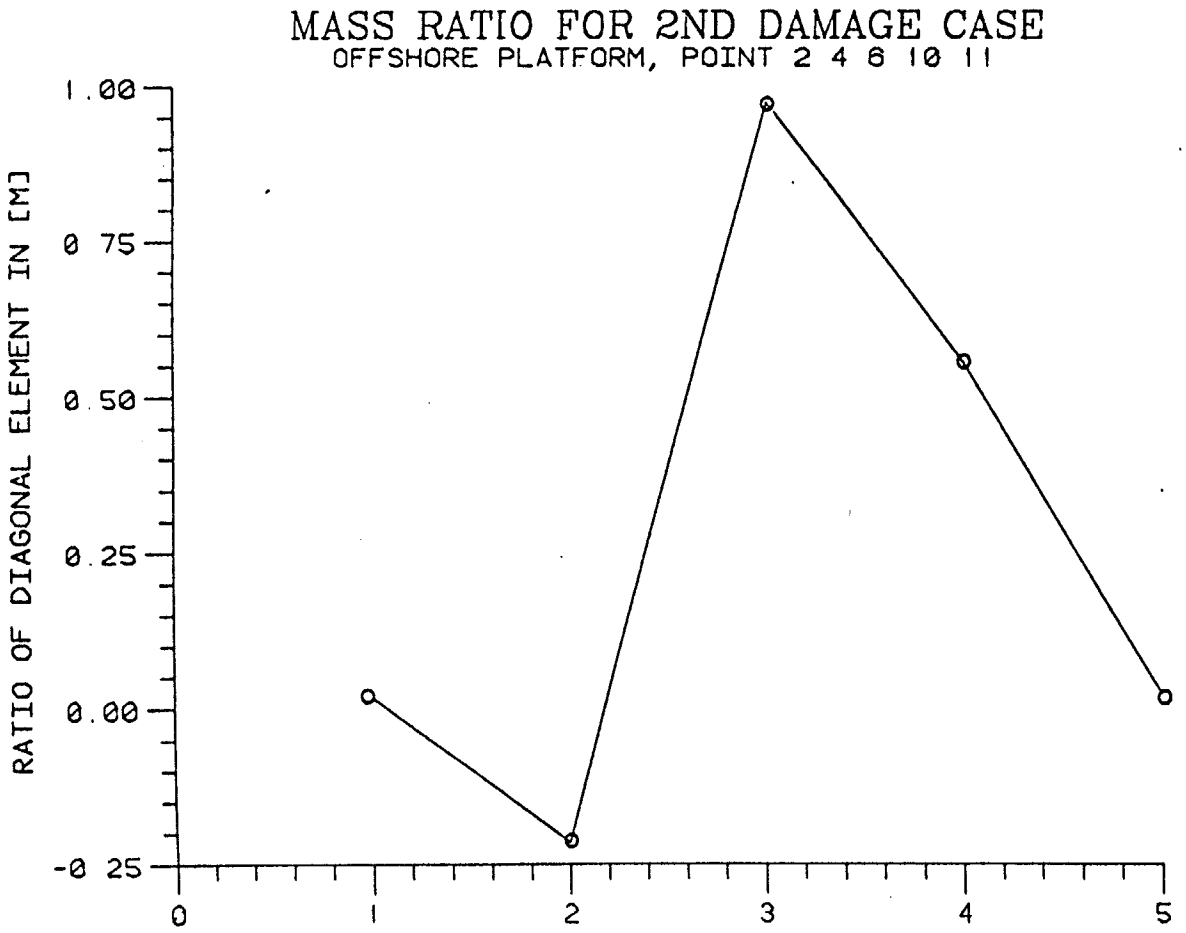

FIG. 49 THE DIAGONAL TERMS IN MASS RATIO MATRIX FOR THE SECOND DAMAGE CASE OF 1/14 SCALE OFFSHORE PLATFORM EXPERIMENTAL MODEL WITH CONCRETE FOUNDATION

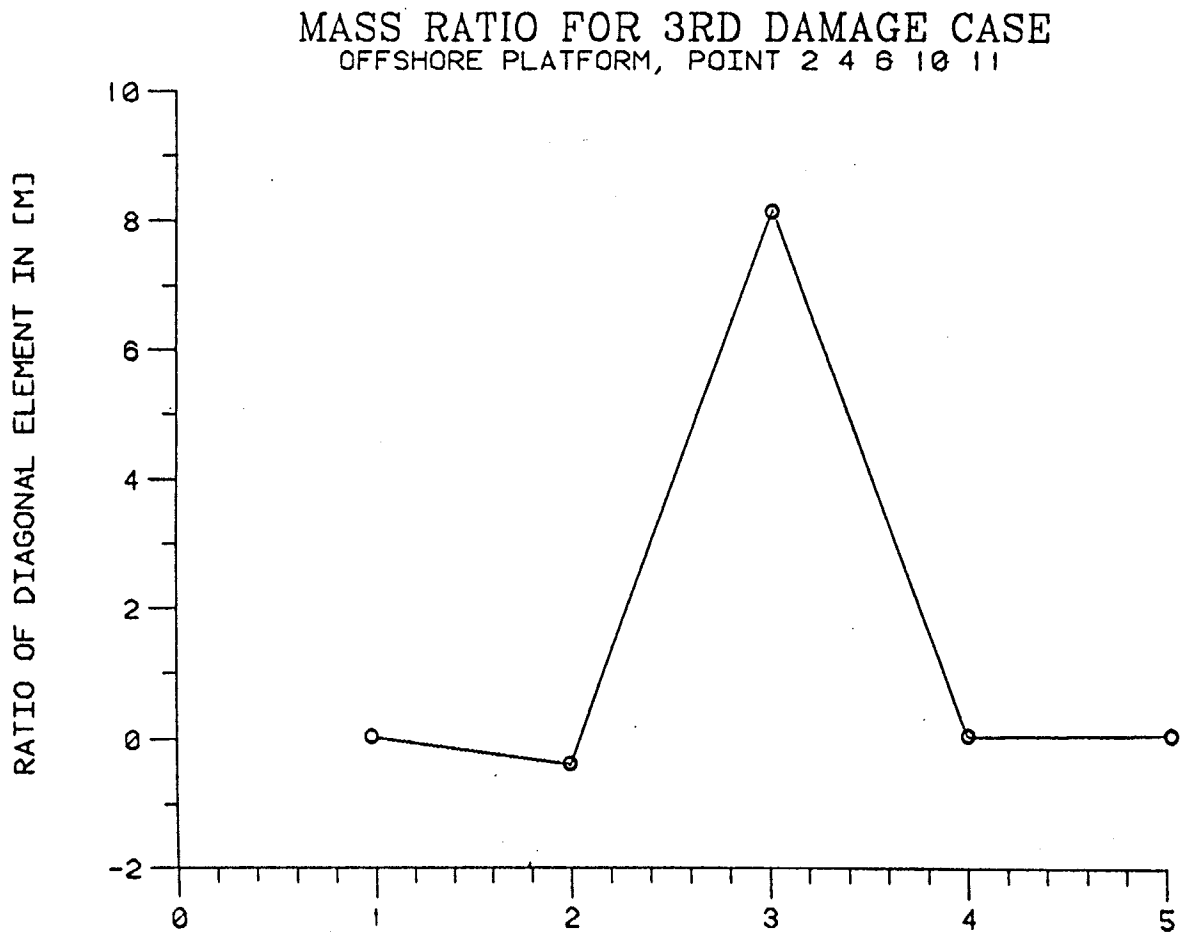

FIG. 50 THE DIAGONAL TERMS IN MASS RATIO MATRIX FOR THE THIRD DAMAGE CASE OF 1/14 SCALE OFFSHORE PLATFORM EXPERIMENTAL MODEL WITH CONCRETE FOUNDATION

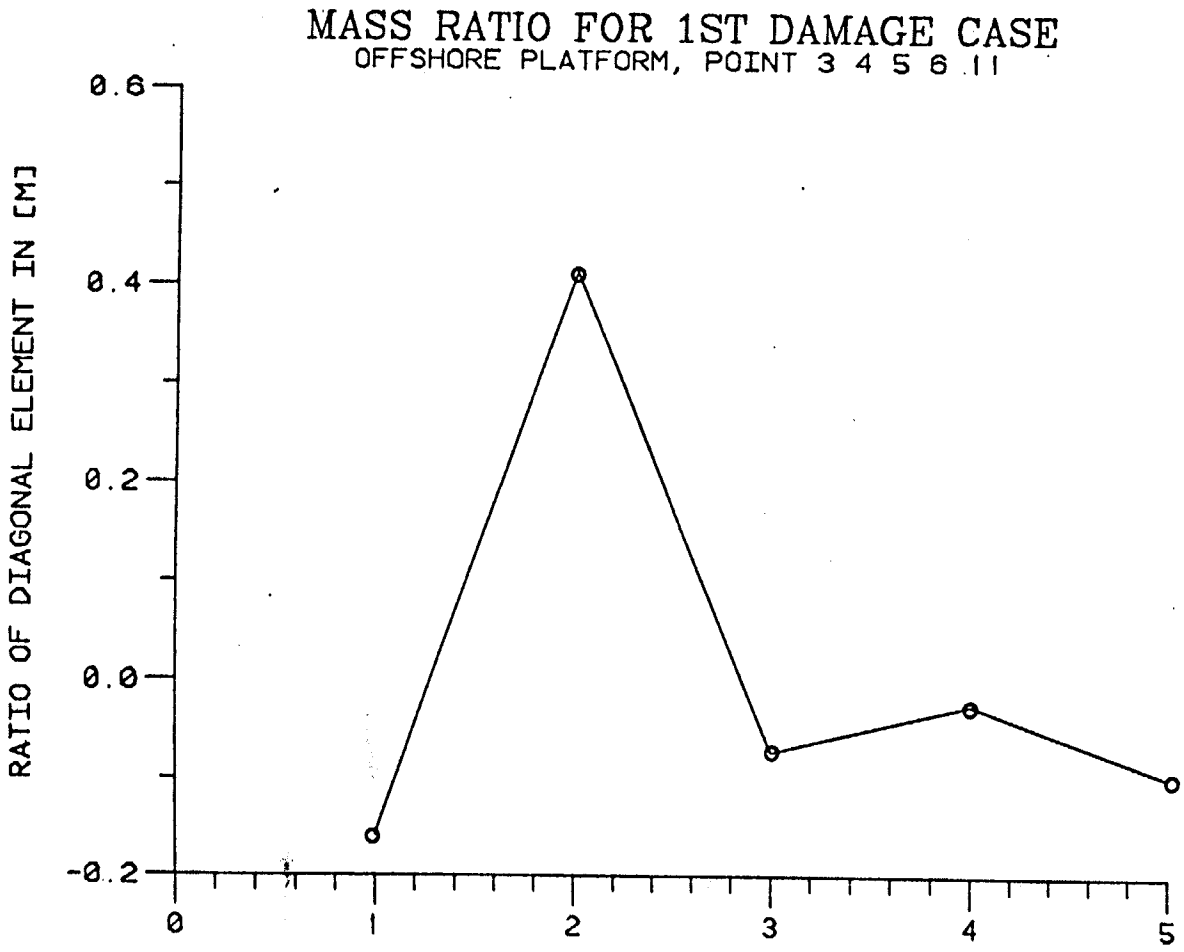

FIG. 51 THE DIAGONAL TERMS IN MASS RATIO MATRIX FOR THE FIRST DAMAGE CASE OF 1/14 SCALE OFFSHORE PLATFORM EXPERIMENTAL MODEL WITH CONCRETE FOUNDATION (THE MODEL WITH POINTS 3,4,5,6 AND 11)

Let us begin by considering a structural system which can generally be represented by an N degree-of-freedom linear system. The dynamics of the system are governed by its equation of motion:

$$[M]\,[\ddot{X}] + [C]\,[\dot{X}] + [K]\,[X] = [f] \qquad \text{- - - - - - - - - - - - - (A.1)}$$

where $[X]$, $[\dot{X}]$, $[\ddot{X}]$ are the displacement, velocity, and acceleration column vectors of the degree of N, respectively. Force column $[f]$ is at the N degree. The $[M]$, $[K]$, and $[C]$ are N x N mass, stiffness, and damping matrices, respectively.

The system identification technique involves the identification of $[M]$, $[K]$, and $[C]$ matrices of the system, from the known responses $[X]$, $[\dot{X}]$, $[\ddot{X}]$ and the known forcing function $[f]$.

Adding to the equation (A.1) a trivial differential equation:

$$[M]\,[\dot{X}] - [M]\,[\dot{X}] = 0 \qquad \text{- - - - - - - - - - - - - (A.2)}$$

a set of equations which describe the motion of the same structural system were obtained:

$$\left[\begin{array}{c|c} [0] & [M] \\ \hline [M] & [C] \end{array}\right] \left[\begin{array}{c} \ddot{X} \\ \hline \dot{X} \end{array}\right] + \left[\begin{array}{c|c} [M] & [0] \\ \hline [0] & [K] \end{array}\right] \left[\begin{array}{c} \dot{X} \\ \hline X \end{array}\right] = \left[\begin{array}{c} 0 \\ \hline f \end{array}\right] \qquad \text{- - - - - - - (A.3)}$$

or in the condensed form:

$$[D]\,[\dot{q}] + [E]\,[q] = [Q]$$

where the matrices are defined as:

$$[D] = \frac{[O]|[M]}{[M]|[C]}$$

$$[E] = \frac{-[M]|[O]}{[O]|[K]} \qquad \text{- - - - - - - - - - - - - - (A.4)}$$

$$[\dot{q}] = \begin{bmatrix} \ddot{X} \\ \dot{X} \end{bmatrix}, \quad [q] = \begin{bmatrix} \dot{X} \\ X \end{bmatrix}, \quad [Q] = \begin{bmatrix} 0 \\ f \end{bmatrix}$$

After performing the Laplace transformation, the following is obtained:

$$[B(s)]\,[q(s)] = [Q(s)] \qquad \text{- - - - - - - - - - - - - - (A.5)}$$

where

$[B(s)] = \left[[D]_s + [E]\right]$ is the system matrix.

It can be proved that [D] and [E] can be represented by the eigenvalues R_k, and eigenvectors $[Y_k]$, produced from the system matrix and determined by the homogeneous equation:

$$[B(P_k)]\,[Y_k] = 0 \qquad \text{- - - - - - - - - - - - - - (A.6)}$$

When [M], [K], and [C] are symmetric, the following expressions

can be proved:

$$[D] = [Y]^{-1T}[I]\,[Y]^{-1}$$
$$[E] = [Y]^{-1T}[-P]\,[Y]^{-1} \qquad \text{- - - - - - - - - - - - - (A.7)}$$

where

$Y = [y_1, y_2, y_3, ---, y_N]$ is an eigenvector matrix

while the eigenvalues matrix is:

$$P = \begin{bmatrix} p_1 & o \\ o & p_2 \\ \hline o & o \\ & & p_n \end{bmatrix}$$

It can be shown that the system's transfer function could be represented as a function of eigenvalues and eigenvectors, that is:

$$[H(s)] = [Y][Is-P]^{-1}[Y]^{T} = \sum_{k=1}^{N} \left[\frac{y_k y_k^{T}}{s-p_k} + \frac{y_k^{*} y_k^{*T}}{s-p_k^{*}} \right] \qquad \text{- - - - - - - (A.8)}$$

or

$$[H(s)] = \sum_{k=1}^{2n} \frac{[a_k]}{s-p_k}$$

where p_k = kth root of {det (B(s)) = 0}

$[a_k]$ = residue matrix for the kth root

APPENDIX II

FREQUENCY DOMAIN CURVE FITTING METHOD

The relation between the ideal and the measured frequency response of a system can be expressed in the following equation

$$g(j\omega) - z(j\omega) = \varepsilon(j\omega) \tag{1}$$

where $z(j\omega)$ is the measured data, $\varepsilon(j\omega)$ is the measurement noise and $g(j\omega)$ is the ideal frequency response.

Assume the system is linear and the transfer function is

$$g(j\omega) = \frac{a_1+a_2(j\omega)+ \ldots +a_{n+1}(j\omega)^n}{b_1+b_2(j\omega)+ \ldots +b_m(j\omega)^{m-1}+(j\omega)^m} = \frac{n(j\omega)}{d(j\omega)} \tag{2}$$

where n and m are assumed to be known ($n \leq m$)

Given a set of measurements, $z(j\omega_k) = \alpha_k + j\beta_k$, ($k = 1, 2, \ldots s$), s is the measured frequency points. The purpose is to estimate coefficients a_i and b_i in (2) by minimizing some cost function of $\varepsilon(j\omega_k)$. Combining Eqs. (1) and (2), one can obtain

$$n(j\omega_k) - [\alpha_k + j\beta_k] \cdot d(j\omega_k) = \varepsilon(j\omega_k) \cdot d(j\omega_k) \quad (k=1,2,\ldots,s) \tag{3}$$

With the definition of the following

$$x = [a_1 \; a_2 \ldots a_{n+1} \; b_1 \; b_2 \ldots b_m]^T$$

$$P_k = [(j\omega k)^0 \; (j\omega k)^1 \; (j\omega k)^2 \ldots (j\omega k)^n]^T = P_kR + j P_kI$$

$$q_k = [(j\omega_k)^0 \; (j\omega_k)^1 \; (j\omega_k)^2 \ldots (j\omega_k)^{m-1}]^T = q_kR + j q_kI$$

Eq. (3) can be rewritten in a matrix form as

$$A_k x - y_k = e_k \quad (k = 1, 2, \ldots, s) \tag{4}$$

where

$$A_k = \begin{bmatrix} P_k R^T & -\alpha_k q_k R^T + \beta_k q_k I^T \\ P_k I^T & -\alpha_k q_k I^T - \beta_k q_k R^T \end{bmatrix} \quad 2x(m+n+1)$$

$$y_k = \begin{bmatrix} \mathrm{Re}\left[(\alpha_k + j\beta_k).(j)^m\right] \\ \mathrm{Im}\left[(\alpha_k + j\beta_k).(j)^m\right] \end{bmatrix} \cdot \omega_k^m \quad 2x1$$

$$e_k = \begin{bmatrix} \mathrm{Re}\left[\varepsilon(j\omega_k).d(j\omega_k)\right] \\ \mathrm{Im}\left[\varepsilon(j\omega_k).d(j\omega_k)\right] \end{bmatrix} \quad 2x1$$

Eq. (4) can be further condensed and written as

$$Ax - y = e \tag{5}$$

where

$$A = [A_1^T\ A_2^T \ldots A_k^T \ldots A_s^T]^T$$
$$y = [y_1^T\ y_2^T \ldots y_k^T \ldots y_s^T]^T$$
$$e = [e_1^T\ e_2^T \ldots e_k^T \ldots e_s^T]^T$$

With least-squares approach one can find the best estimate of x for Eq. (5) that minimizes the following cost function

$$E_0 = ||e||^2 = \sum_{k=1}^{s} |\varepsilon(j\omega_k)d(j\omega_k)|^2 \tag{6}$$

is

$$x = (A^T A)^{-1} A^T y \tag{7}$$

This is, in fact, the same result as what Levy got in (17).

Instead of eliminating the weighting factors, $d(j\omega_k)$ in Eq. (6) as what others did (18-20), a new set of weighting facators is introducted here into Eq. (6) through iterations. The procedure is as follows.

1. Let $n(j\omega_k)_L$ and $d(j\omega_k)_L$ be the values of $n(j\omega_k)$ and $d(j\omega_k)$, respectively, based on the estimate of x in the L-th iteration.

2. Replace $n(j\omega_k)$ and $d(j\omega_k)$ with $n(j\omega_k)_L$ and $d(j\omega_k)_L$, respectively, in Eq. (3) and divide both sides by $n(j\omega_k)_{L-1}$ to yield

$$\frac{n(j\omega_k)_L - z(j\omega_k)d(j\omega_k)_L}{|n(j\omega_k)_{L-1}|} = \frac{\varepsilon(j\omega_k)d(j\omega_k)_L}{|n(j\omega_k)_{L-1}|} \qquad (8)$$

3. Rewrite eqn. (8) in matrix form as

$$D_k A_k x_L - D_k Y_k = D_k e_k \quad (k = 1, 2, \ldots s) \qquad (9)$$

where

$$D_k = \frac{1}{|n(j\omega_k)_{L-1}|} \begin{bmatrix} 1 & 0 \\ 0 & 1 \end{bmatrix} \qquad (k= 1, 2, \ldots s)$$

4. Combine all equations in Eq. (9) together in the following matrix equation,

$$DAx_L - Dy = De \qquad (10)$$

where

$$D = \begin{bmatrix} D_1 & & 0 \\ & \ddots & \\ & & D_k \\ & \ddots & \\ 0 & & D_s \end{bmatrix}$$

5. Formulate the new cost function as

$$E_1 = \|De\|^2 = \sum_{k=1}^{s} \left| \varepsilon(j\omega_k) d(j\omega_k)_L / n(j\omega_k)_{L-1} \right|^2 \qquad (11)$$

6. Obtain the best estimate of x_L for the L-th iteration

$$x_L = (A^T Q A)^{-1} A^T Q y \qquad (12)$$

where $Q = D^T D = D^2$

To initiate the procedure, or equivalently for L = 1, one can assume $|n(j\omega_k)_0| = 1$, which will give Levy's result of a_i's as the result of the first iteration.

APPENDIX III

SOIL MODELLING

The spring constant to simulate the Winkler foundation was given by Haldar (1977), reference (43).

$$K_i(z) = K_c(z)\, S_i$$

$$K_c(z) = \frac{8\pi}{3} E(z) \left\{ \sinh^{-1}\frac{h-z}{r} + \sinh^{-1}\frac{h+z}{r} + \frac{2}{3r^2}\left[\frac{r^2h - 2r^2z + hz^2 + z^3}{\left[r^2+(h+z)^2\right]^{1/2}} - \frac{-2r^2z + z^3}{\left[r^2+z^2\right]^{1/2}} \right] - \frac{2}{3}\left[\frac{z-h}{\left[r^2+(h-z)^2\right]^{1/2}} - \frac{z}{\left[r^2+z^2\right]^{1/2}} \right] + \frac{4}{3}\left[\frac{r^2z + hz^2 + z^3}{\left[r^2+(h+z)^2\right]^{3/2}} - \frac{r^2z + z^3}{\left[r^2+z^2\right]^{3/2}} \right] \right\}^{-1}$$

where $K_i(z)$ is the i-th spring constant, S_i the i-th spacing, h the height of the pile, r the radius of the pile, and z the soil depth. E(z) is the Young's Modulus at depth z , and is derived from the shear modulus, G , which is expressed as the following formula

$$G = 1000\, K_2\, (\sigma_m')^{1/2} \text{ (psf)}$$

σ_m' = average of three principal stresses = $\dfrac{\sigma_1 + \sigma_2 + \sigma_3}{3}$

$\sigma_1 = \gamma z$

γ = soil weight density 100 lb/ft^3 (assumed)

$\sigma_2 = \sigma_3 = k_0 \sigma_1 = (1-\sin\phi)/(1+\sin\phi) \cdot \sigma_1$ (for cohesionless soil) (44)

ϕ = soil friction angle from triaxial test = 30^0 (assumed)

k_2 = 50 (assume soil is in low strain level (10^{-4}))

$K_c(z)$ is derived from the Mindlin equation which gives the horizontal displacement as induced by a single concentrated force located at any point within an isotropic half-space and exerting in horizontal direction.(45)

The more detailed explanation for the above equations can be found in reference (46).

REFERENCES AND REPORTS

1. Kummer, E.; Yang, Jackson C.S.; Dagalakis, Nicholas G.; "Detection of Fatigue Cracks in Structural Members," 2nd American Society of Civil Engineering/EMD Specialty Conference, Atlanta, Georgia, Jan. 15-16, 1981, Proceedings, pp 445-460.

2. Yang, Jackson C.S.; Chen, J.; Dagalakis, Nicholas G.; "Damage Detection in Offshore Structures by the Random Decrement Technique," 2nd International Offshore Mechanics and Artic Engineering Symposium, 1983.

3. Yang, Jackson C.S. et. al; "Measurement of Structural Damping Using the Random Decrement Technique," 53rd Shock and Vibration Symposium, New Orleans, La., April 1982, and Shock and Vibration Bulletin, Vol. 53, May 1983.

4. Tsai, T.; Yang, Jackson C.S.; Chen, R.Z.; "Detection of Damages in Structures by the Cross Random Decrement Method," 3rd Arctic Modal Analysis Conference, Jan. 1985, Orlando, Florida.

5 Tsai, W.H.; Yang, Jackson C.S.; "Damage Detection and Location in Complex Structures," ASME Design Engineering Technical Conference, Sept. 10-13, 1985, Cincinnati, Ohio.